Towards More Accurate Medical Simulation via Procedural Instrumentation

A THESIS
SUBMITTED TO THE FACULTY OF THE
UNIVERSITY OF MINNESOTA
BY

Amer Safdari

IN PARTIAL FULFILLMENT OF THE REQUIREMENTS
FOR THE DEGREE OF
MASTER OF SCIENCE

Timothy M. Kowalewski

July, 2019

Acknowledgements

There are many people that have earned my gratitude for their contribution to my time here at the University of Minnesota, and here I'll do my best to list a few examples in chronological order. This is by no means a complete list; it takes a village (faculty, colleagues, friends) to raise a child (my curiosity for science, medicine, and engineering).

First off I'd like to thank Fluvio Lobo, without him I would simply not have the passion and curiosity for research that I do now and its all thanks to his mentorship early in my academic career. Next I'd like to thank professors Barocas, Alford, Wood, Johnson, Netoff and all the BME faculty members who have trained and moulded me into the engineer I am today. Cole Nielson deserves a special thanks for spoon feeding me all of my knowledge of circuit theory, but more importantly, the practical parts that are conveniently left out of undergraduate education.

I am also deeply indebted to Prof. Tim Kowalewski for agreeing to mentor and fund my graduate education. In hindsight I often did not deserve that privilege, and our work together has been a road paved with many bumps and potholes along the way, but without him taking a chance on me – I would honestly not have had the opportunities I needed to struggle and grow. Without his mentorship and guidance, I would likely not have made it into medical school to pursuit my dream of marrying engineering and medicine.

Lastly I'd like to thank my colleagues for their support over the years. Trevor Stephens was often the guiding hand when I had no idea what to do next. Jayme Lee and Celeste Blum were often the two that kept the lab fun when the work itself might not have been as exciting. And a final thanks to the rest of my lab mates who volunteered their time, directly or indirectly, to helping me and my project.

Dedication

I would like to dedicate this work to my wife Mehreen. Without her I simply would not be the man I am today. I also would not be nearly as well dressed as I sometimes am without her insight.

Abstract

By 2030, the United States will find itself short of almost 100,000 physicians to care for its population. This has significant implications not only for patients, hospitals, and health care providers around the country – but also for educators. The objective of this thesis, in a broad sense, is to explore techniques and science needed for more accurate surgical simulation. More specifically, the particular niche that has been carved out by my work as a Masters student is quantifying the change in tissue properties between the in-vivo tissues that physicians work with, and the ex-vivo tissues that biomechanicians commonly study due to convenience. The implications of this work will hopefully help drive the development of more accurate next generation medical simulators. A prototype device design, experimental protocol, and data analysis strategy is proposed to quantify the change in in-vivo to ex-vivo tissue response. This is validated on n = 4 porcine carcasses and lays the groundwork for an imminent n = 5 in-vivo porcine study. The last chapter of this thesis presents another avenue of improving medical simulators, by providing a case study on the kinematic assessment of urinary catheterization. The unifying theme consists of introducing technologies for procedural instrumentation to bring more quantitative rigor to surgical science.

Contents

List of Tables

List of Figures

Chapter 1

Introduction

1.1 Motivation

The Association of American Medical Colleges (AAMC) estimates that by 2032 the United States will have a shortage of over 100.000 physicians [3]. This issue needs to be tackled on two fronts, the first of which is with regards to changes in public policy which is out of scope for a masters thesis in biomedical engineering. The other course of action needed to address this issue is to invest in improving medical education. Medical institutions around the world are turning towards simulation technologies to educate the next generation of physicians. More accurate simulators will minimize the adjustment and time needed for student doctors to transfer their training from simulator to patient. Higher fidelity simulators will also have the effect of improving clinical care, and reducing error rates caused by novice physicians.

A key limitation in current medical simulators is that a vast majority of them do not properly mimic the responses of a living human patient, which leads to a need to unlearn bad behaviors or in other words, negative training transfer [Fig. 1.1]. There is healthy progress in improving these simulators using existing data on tissues [Fig. 1.2]. There is a considerably body of literature in biomechanics dedicated to characterizing tissue properties. Unfortunately, most of this work is done outside the natural environment of the tissue after the host has deceased. For simulators, ex-vivo tissue data is one step forward in accurately reproducing real world behavior; however, the ultimate goal is to use models generated from in-vivo tissues. One first step in addressing this issue,

Figure 1.1: Example of a medical simulator used for airway trauma [Trucorp, Co.Armagh, N. Ireland]. The bulk of mannequins such as these are typically made using tough plastics and/or silicones due to their ease in manufacturing and cost, with more attention given to the particular anatomy or procedure the simulator is intended for. This approach is still largely inadequate to provide the proper training transfer needed to be successful in a patient setting.

Figure 1.2: Example of a high fidelity medical simulator [Syndaver Labs, Tampa, FL]. These simulators are significantly more expensive but they often pay much greater attention to detail to emulating the characteristics of actual tissues.

to bridge the gap between in-vivo properties and ex-vivo, is to simply characterize the discrepancy in mechanical response response. This initial approach has one significant advantage, in that characterizing the discrepancy will allow the preexisting body of literature to remain useful for simulator design. Additionally, if it turns out that in-vivo tissues are not drastically different than ex-vivo tissues, then this work would validate existing literature and provide assurance to future work that the measured properties are indicative of what would be encountered in a clinical setting.

Studying tissue responses and using mathematical models to characterize their behavior is a fundamental, and necessary science to produce highly realistic simulators. Another approach that yields approximate results, without the level of complexity required in characterizing tissue responses, is to experimentally measure the mechanics of each procedure one wishes to model with a simulator. The key limitation in this approach is that the upfront complexity in modeling is obviated at the cost of losing generalizability and interpretability. Not only does each procedure or surgical act need to be measured separately, but the resulting data (typically forces and motions) does not directly inform the required stiffnesses or parameters of the various silicones/polymers; forcing simulation scientists into a trial and error approach to match the simulator to the experiment. Both approaches are useful to advance in parallel for the development of next generation medical simulators. Given the importance of procedure-specific characterization, chapter 5 of this thesis presents preliminary cadaveric work in measuring the mechanics of urethral catheter insertion.

1.2 Research Objectives

The ultimate objective of this research is to measure and compare the mechanical response of porcine tissues from *in-vivo* to *ex-vivo* across common testing modalities. The organs of interest to this study are those commonly encountered in surgical simulators. Comparing *in-vivo* mechanical data relative to data collected by common *ex-vivo* testing protocols will help clarify two concepts hindering accurate surgical simulators: which currently existing ex-vivo tissue data, if any, are reasonably accurate for use in surgical simulation, and how much discrepancy is there between testing *in-vivo* and *ex-vivo* for each of these organs. This study was conducted by collecting data from a

custom hand held grasping tool on porcine liver and spleen. The force displacement data was analyzed both using a model free, data driven approach and also by applying traditional finite element modeling.

Due to scheduling and regulatory conflicts, the in-vivo data could not be measured in time for this specific thesis. However, this thesis will serve as a blueprint for conducting the in-vivo collection by outlining and validating the device design and experimental protocol that can be used to conduct a successful in-vivo experiment. The device and protocol described in the coming chapters will be validated on ex-vivo porcine in-situ, which should be sufficient for predicting viability of an in-vivo study.

1.3 Literature Review

The purpose of this literature review is to provide a brief overview of the present work regarding the mechanical characterization of in-vivo tissues. The structures of interest are mainly soft body organs such as the liver, kidney and etc. Included in the scope of this work is a brief discussion of the state-of-the-art mathematical models currently used to describe bulk tissues in-vivo.

One of the first direct comparisons between in-vivo and ex-vivo tissue was conducted by Rosen et al. [17]. This paper tested and compared the mechanical properties in-vivo and ex-vivo of porcine soft organs. The purpose was to rectify the discrepancies between mechanical properties measured ex-vivo verses the actual properties present in-vivo. One motivation for this work is for the development of mechanically accurate medical simulators for training new surgeons.

Rosen et al. developed a handheld grasping device (MEG) which imposes similar compressive loads as in surgical procedures; this device has sensors to calculate stresses and strains. The MEG device was novel in the sense that it can gather data in-vivo; most biomechanical research focuses on ex-vivo tissue. The data collected with the MEG device was compared with a commercial uniaxial compressive fixture (MTS) which is commonly used in biomechanical research. The MTS fixture could only be used to measure the properties of organs ex-vivo.

For in-vivo experimentation, the porcine animals were sedated and setup in a similar

fashion that is used when training laparoscopic surgeons. One key deviation from standard biomechanical protocol is the omission of tissue preconditioning. Preconditioning was omitted with the justification that patient tissue during surgery will almost never be "preconditioned"; preconditioning would make the extracted properties not clinically relevant. Following the in-vivo tests, the animal was sacrificed and ex-vivo tests were immediately performed. The typical justification for preconditioning is that it significantly reduces the variability in the data. For mechanical tests, a stress-relaxation and cyclic loading strain waveform was used. The data collected was fit with a phenomenological modeling approach. Their key finding was that the properties of the tissue are different in-vivo vs ex-vivo for most organs. For most organs the in-vivo stresses were higher at a given strain than when tested ex-vivo. The key limitation to their study is that their modeling was purely a curve fitting approach with no regard for physical meaning. A constitutive modeling approach would provide greater insight. In addition, this work did not track the profile for how the tissue properties change over time postmortem.

Transitioning away from soft organ biomechanics. Mazza et al. perform some initial work on testing the mechanical properties of the human cervix both in-vivo and ex-vivo before/after a hysterectomy procedure [10]. They used a stiffness parameter to characterize each experimental trial; the data was collected using an aspiration experiment. Unfortunately, they did not find any statistically significant difference between ex-vivo and in-vivo cervical tissue when exposed to the aspiration experiment. They authors cite that the lack of a difference could potentially be masked by the variability of the data.

Ocal et al. demonstrated that bovine liver tissue gets stiffer and more viscous the longer it is preserved ex-vivo [15]. They used 2 independent tests to extract the material properties: an impact test for storage and loss moduli and a stress relaxation rest for the relaxation modulus. The data from these two experiments fed into a generalized maxwell model ($n = 3$ was found to be optimal). Tissue was tested in this fashion at various time points ranging from 1 hour to 24 hours postmortem The storage, loss, and relaxation moduli for the tissue was observed to increase with preservation time; this indicates that the tissue is stiffer and more viscous. One limitation of this paper include a lack of testing in-vivo or even on fresh excised tissue immediately postmortem. In addition, as the authors point out, their use of a linear viscoelastic model does not take

material nonlinearities and rate dependent effects into account.

Kerdok et al. investigated the importance of perfusion on the mechanical properties of the liver using a porcine model [7]. Cyclic and creep indentation experiments were performed under 4 different conditions: in-vivo, ex-vivo perfused, ex-vivo post perfused, and in-vitro on an excised section at small and large strains. The viscoelastic properties of the liver were fit using a linear 1st and 2nd order Kelvin-Voigt/Maxwell style model. The authors demonstrated that the in-vivo and ex-vivo perfused tissue behaved significantly different than ev-vivo post perfused and in-vitro tissue. The in-vivo and ex-vivo samples had similar viscoelastic properties with some slight deviation. The authors attribute these discrepancies as a mismatch in the perfusion pressures and concentration; they mention that finer tuning may lead to a closer in-vivo to ex-vivo match. Another point made is that the tissue samples that were tested were also sent to histology to determine the extent of damage. The histologist reported little to no damage which may provide evidence that the perfusion kept the tissue mechanically preserved. One remaining challenge the authors noted is to replicate the in-vivo boundary conditions for ex-vivo experimentation. In addition, accounting for the internal stress state in-vivo is necessary for developing a constitutive model.

Brouwer et al. conducted mechanical experiments on tissue in-vivo and ex-vivo on porcine [1]. Their motivation was to provide accurate haptics for surgical simulation. A table mounted fixture was developed which could measure tensile properties; a indentation device was used to compress tissues that were too fragile for a tensile test. In addition, Brouwer et al. rigged sensors to common surgical equipment and measured the forces/torques while surgical residents performed various tasks. They fit their data to a simple exponential curve and saw very good agreement. The fit parameters were different for in-vivo vs ex-vivo. This discrepency is attributed to the change in boundary conditions from their in-vivo to ex-vivo experimental procedure. Limitations of their work include the lack of a constitutive model, and a lack of relatability between in-vivo to ex-vivo experiments. Brouwer et al. mentions that finite element simulations may bridge this gap.

Nava et al. perform mechanical characterization of human liver tissue in-vivo during open surgery using an aspiration experiment [13]. An inverse finite element calculation was used to determine the parameters for a QLV model and a Robin-Bodner nonlinear

elastic-viscoplastic model. Both models fit rather well; the Robin-Bodner has better predictive power for repeated loading cycles. The main experimental limitation of this study was the initial applied pressure on the aspiration instrument by the surgeon. This initial pressure could not be adequately controlled for and the authors indicate that their reported results likely overshoot the true material stiffness by roughly 10

Miller develops a linear viscoelastic constitutive model and applies it to the compression of brain tissue [11]. The experimental data was fit by continually adapting parameters of a finite element model until the parameters converged. Their parameter fit did quite a good job of modeling the experimental data; however, the error in their model was largest at the slowest strain rate indicating that the model may not be complete.

In a subsequent paper, Miller et al. compared compression data from an in-vivo porcine experiment to the constitutive model generated with ex-vivo data [12]. In the experiment, a porcine brain was exposed and an indentation test was performed to 3.9 mm. The brain was excised and scanned via MRI; the MRI image was used to construct a finite element mesh. The experiment was simulated in-silico using the model parameters for a hyperelastic, linear viscoelastic constitutive model. The model captured the general trend of the in-vivo dataset, however the error was up to 33%. The authors indicate that the parameters could be updated to better fit the data - but never do so in the actual paper.

Samur et al. tested porcine liver in a minimally invasive fashion by using laparoscopic ports to guide an indentation instrument [19]. An inverse FE simulation was used to extract material properties for a Mooney-Rivlin model. Lim et al. characterizes cadaveric soft tissue using a robot retro-fitted for indentation testing [8]. The stress strain data is fit to many different models including a Fung QLV model. A few shortcomings of their work include the use of preconditioning, and a lack of experimental validation using FE simulations.

Zhang et al. uses a Rubin-Bodner model with a Generalized Regression Neural Network (GRNN) to predict the facial structure of a patient following a CMF surgery [21]. This was a retrospective study that used patient specific facial scans and fed the mesh into an FE simulation using the RB model without the short-term viscous terms. According to the authors the results were quite good, they were able to better

plan CMF surgeries to achieve a desired facial structure. The relevance of this paper is the prediction of in-vivo, biomechanical deformations by combining a sophisticated constitutive model with a machine learning approach to improve accuracy.

Boonvisut et al. developed a framework to characterize soft tissue properties in real time from a robotic manipulator. A camera system tracks markers on the object of interest to generate estimates of the strain field. The geometry of the object is known a priori, and the stresses are determined from the force at the robot manipulator. The information from these 3 sources allow for a inverse finite element model to back calculate the relevant material properties for any constitutive model (neo-hookean was used for this work). Once the material properties are found, the algorithm can then simulate deformations necessary for the robotic trajectory calculations. Limitations of their work include the lack of physically validating their method for complex object geometries and a lack of actual tissue testing.

	Attributes					
Reference	*in-vivo*	*in-situ*	*ex-vivo*	Modeling	Test Specimen	Test Type
Brouwer et al. [1]	✓		✓		porcine organs	tension, indentation
Kerdok et al. [7]	✓		✓	maxwell/voigt	porcine liver	indentation
Lim et al. [8]		✓		quasi-linear viscoelastic	human cadaver stomach	indentation
Mazza et al. [10]	✓		✓		human cervix	aspiration
Miller [11] and Miller et al. [12]	✓		✓	linear visoelastic	porcine brain	indentation
Nava et al. [13]	✓			qlv, robin-bodner, finite element	human liver	aspiration
Nicolle et al. [14]			✓	non-linear viscoelastic	porcine kidney, liver	rotational rheometry
Ocal [15]			✓	maxwell-voigt	porcine liver	impact, stress relaxation
Rosen et al. [17]	✓		✓		porcine organs	compression with surgical grasper
Samur et al. [19]	✓			mooney-rivlin, finite element	porcine liver	indentation, stress relaxation
Proposed Study	✓	✓	✓	mooney-rivlin/ogden finite element and model free	porcine organs	indentation with hand-held grasper device

Table 1.1: Table summarizing the current body of literature

The current body of literature has already explored a vast set of topics. The key area that has not been studied is the unknown gap between ex-vivo and in-vivo tissues. Not only is there tissue decay as seen in Ocal et al. [15], but as mentioned in several papers the boundary conditions in-situ vs ex-vivo can be vastly different [17], [7]. There is a lack of literature which quantifies the discrepancy between the properties canonically measured ex-vivo, and the true properties in-vivo. Rosen and Miller have started this work back in the 2000s and since then no new papers have surfaced which attempt to explain the observed differences between in-vivo and ex-vivo tissues using a constitutive modeling approach.

1.4 Organization and Content

This thesis starts with the development of a platform (hardware and software) that can be used to reliably measure tissue response both in-vivo on an operating table, and ex-vivo on a lab bench. This platform was then used on n = 4 porcine carcasses to validate its suitability for use in a future n = 5 in-vivo study. This thesis' primary deliverable is the analysis of the n = 4 dataset, which will serve the basis for the analysis in the future study which we intend to publish to a peer-reviewed journal.

Chapter 2

Device Design: Hardware and Software

This chapter presents the bulk of the design process that culminated into the final device suitable to conduct the proposed experimentation. The design requirements are outlined, followed by a brief discourse into the initial device designs that were deemed unsuitable. The last section describes the hardware and software that was used in the final iteration of the device.

2.1 Design Requirements

The design requirements were primarily driven by the need for a testing methodology that would yield consistent results between experimental conditions. Common mechanical testing methodologies such as tension (uniaxial/biaxial) and compression (free/confined), while incredibly robust and ubiquitous, were deemed unsuitable due to the difficulty of being able to implement and replicate the exact same testing conditions on the lab bench as well as in-vivo e.g. capturing or controlling the boundary conditions between cases is forbiddingly impractical. With suitability in-vivo as the primary criteria in mind, the following list contains a set of guiding criteria used when evaluating and designing potential device candidates.

- Required Characteristics

  - Suitability for minimally invasive access in-vivo
  - Accurate, precise measurement of a force-position response in specimen tissue, that can be correlated to some notion of stiffness/mechanical property
  - Device measurement is consistent across conditions, i.e. allows for an "apples to apples" for data collected in-vivo and ex-vivo
  - Position measurement derived from a digital encoder source
  - Force measurement has proper analog conditioning and filtering
  - Force and position data streams sampled with a frequency of at least 1 kHz
  - Data streams can be monitored in real time
  - Measurement device and all auxillary components are capable of being sufficiently shielded from tissue matter, or are reasonably distant from the experiment to obviate this concern
  - Calibrated force measurements are accurate to ± 5 mN, position measurements are accurate to ± 1 mm
  - Typical experiments with device do not exceed 20 minutes to conduct a thorough measurement on a single target organ within one experimental condition

- Desired Characteristics
  - Measurement with device is autonomous (motorized), lacking a need for human input in the measurement pipeline
  - Measurement device can be handheld
  - Measurement device can be cleaned in an autoclave
  - Device is wireless

2.2 Unsuccessful Approaches

2.2.1 Grasping with Da Vinci Surgical Tools

One obvious technique for manipulating in-vivo tissues and collecting mechanical data is to exploit existing surgical tools. The primary benefit is that these devices are

Figure 2.1: An example of a Da Vinci Surgical Grasper (Intuitive Surgical, CA).

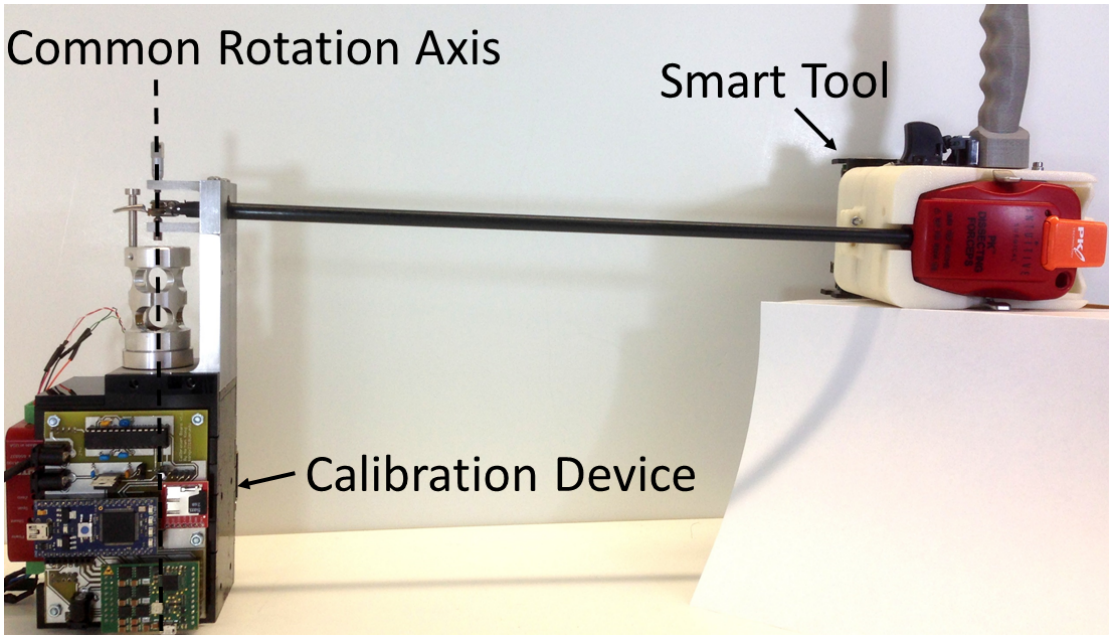

Figure 2.2: Depicts the SmartTool v1 design and calibration fixture. The end effector data collected from the calibration jig was mapped from the sensors on the back end of the Da Vinci grasper using a simple neural network.

already rigorously designed to handle the stresses of anatomical contact and thus are easy to work with and clean. The main disadvantage is that very few surgical tools are intended to be used as a data collection platform. One surgical device that seemed suitable for in-vivo data collection was the graspers on the Da Vinci Surgical Robot [Fig. 2.1]. Da Vinci surgical robots have found the most success in Urological operations, and in that field they have largely displaced their alternatives such as laparoscopy.

The graspers are primarily actuated using a cable-pulley system along a shaft. Commercially, these devices are not outfitted with sensors on the grasper end effector – instead there are a set of sensors on the back end of the pulley system that measure the current sent to the actuators that pull the spindles. As our first approach, we developed a system that encompasses various Da Vinci graspers, and instrumented them with torque sensors and encoders at the back end spindle. Using this platform which is referred to as the SmartTool, we hypothesized that the mechanics at the back end of the grasper are predictive of the mechanics at the end effector. A calibration jig [Fig. 2.2] was developed to develop this mapping; it turns out a simple neural network with a

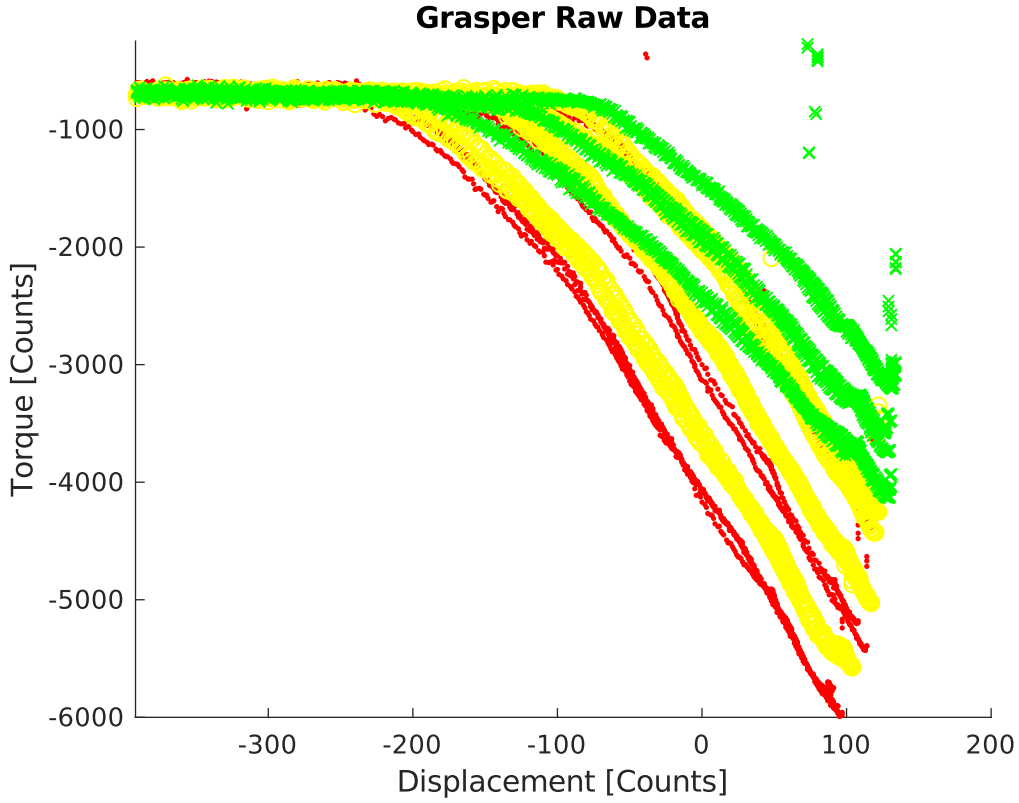

Figure 2.3: Shows raw data from Da Vinci grasper platform. Each color of curve represents a different synthetic material with a unique stiffness – red > yellow > green. Each individual curve is of a given material of a given thickness; there is no normalization for thickness in this plot.

single hidden layer is sufficient to predict end effector torques within 1.07 mNm, and positions (jaw angles) within 0.17°. This completely obviated the need to model the physics of the system which is incredibly complex due to the design of the cable-pulley system that allows the maneuverability needed by surgeons. The success and accuracy from using these Da Vinci graspers on our platform was a key motivator for nominating them for use for the in-vivo data collection.

Fig. 2.3 shows data collected using the SmartTool on synthetics of different stiffnesses (denoted by color), and thickness. This plot does not show any normalization for the thickness of the grasped material. When analyzing the data to normalize for thickness, we encountered a severe issue – the data can be arbitrarily shifted (i.e. a

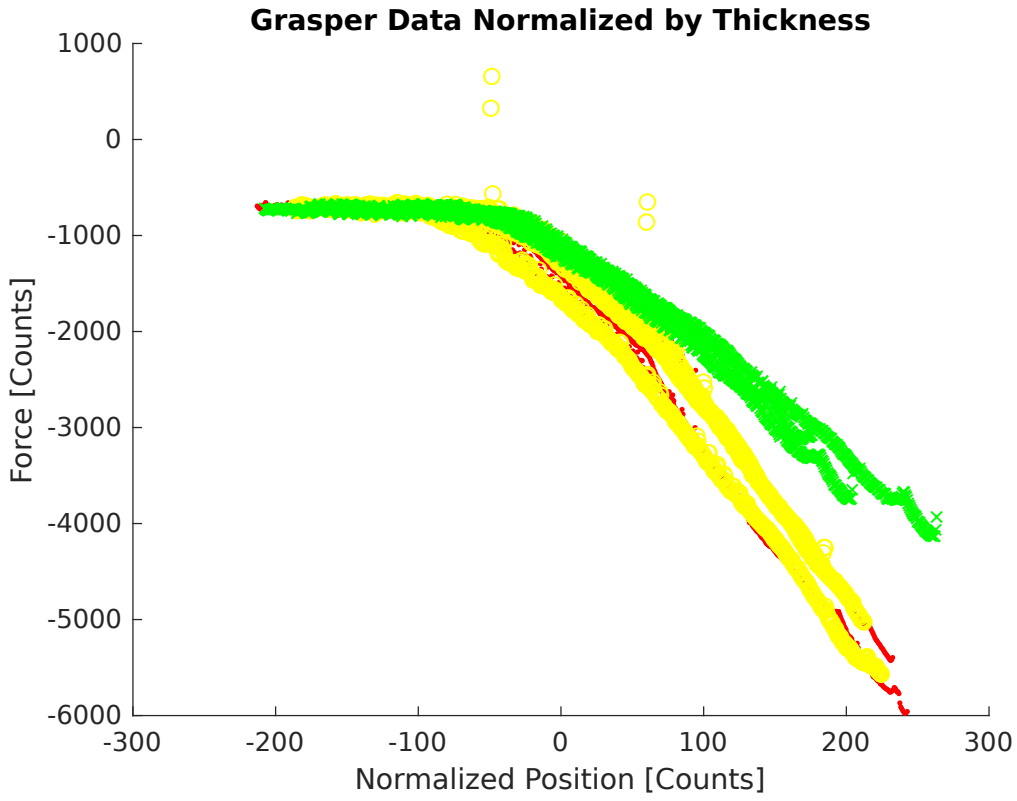

Figure 2.4: Grasper data from the previous figure, with the displacement normalized (i.e. shifted) to account for the difference in material thickness. Each color represents a different synthetic material. The main issue is that the grasper simply cannot distinguish between different mechanical properties.

thickness normalization operation) such that data from different materials gives identical responses. The figure shows data from the yellow and red synthetic yielding a similar mechanical response, giving the wrong implication that the two materials have similar properties. The inability to distinguish between two different materials that have starkly different properties makes this platform unsuitable for the in-vivo experimentation. It is hypothesized that the identical mechanical responses are due to some tension based phenomenon in the cables of the grasper dominating the interaction. This drowns out the effects of the material-tool interaction at the end effector – leading to a lack of discrimination in mechanical responses in the two stiffer synthetics.

2.2.2 Indentation

After discovering critical issues with the SmartTool design that could jeopardize the project deliverables, we turned our attention onto alternative in-vivo mechanical characterization methods. The literature review presented in Section 1.3 suggested that indentation may yield a successful approach. Indentation solves the key issue the SmartTool possessed in that given a sufficiently large and wide enough medium (known as infinite half-space), the force-displacement curve generated from indentation will be geometry independent due to results in contact theory. Thus the data collected will more properly reflect the underlying material properties, instead of being dependent on the material geometry, i.e. thickness. An example of this property of indentation is illustrated in Fig. 2.7. Given the indenter geometry, for "small" displacements, there are analytical solutions for the Young's Modulus and Poisson's Ratio. Additionally, non-linear material parameters can be extracted from indentation using finite element models, which while not completely simple, is a vastly easier problem than modeling the tool-material interaction of the Da Vinci jaw.

The indenter prototype was composed of a P16-50 linear actuator from Actuonix Motion Devices Inc, a linear bearing with custom machined rod, and an aluminum plate that links them together [Figs. 2.5 and 2.6]. All the components are encased in an acrylic box. In front of the aluminum plate is a 5 lb submersible load cell from FUTEK Inc (model LSB210). Attached to the load cell is a custom machined spherical indenter tip with a diameter of 6 mm. A quadrature linear encoder from U.S. Digital is positioned on the rod allowing accurate position measurements. The encoder strip has 500 counts

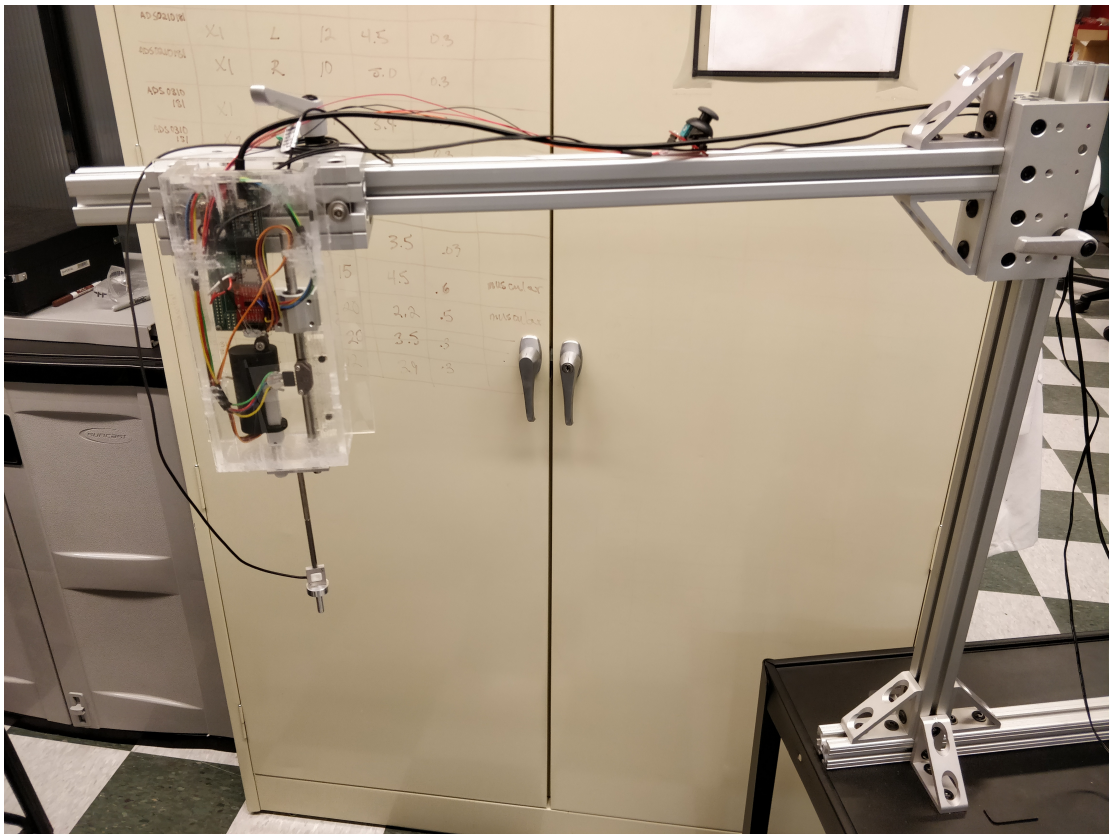

Figure 2.5: Photo of custom indenter prototype mounted onto a cart. The electronics housing contains a DC motorized actuator, a linear encoder, and a linear bearing to maintain alignment between the two. Both the actuator and encoder connect to a baseplate which is offset from the load cell and indenter tip [Fig. 2.6].

Figure 2.6: Close up photo of the spherical indenter tip and load cell (Futek LSB210 submersible load cell).

per inch providing a resolution of roughly 50 micrometers. A custom PCB contains the motor driver, Teensy 3.5 microcontroller, and other associated circuitry to power and collect data from the device. The microcontroller communicates over serial with a PC; the PC sends commands and receives data through a GUI application. The device is capable of acquiring and sending the encoder position data at 3 kHz, but is limited to 80 Hz acquisition for the load cell, therefore time synchronized force-displacement is logged at 80 Hz.

The indenter prototype design was quite successful initially in a pilot study measuring the effects of temperature change on tissue response [Figs. 2.8 and 2.9]. Fresh (roughly 24 hours post-mortem) porcine tissue was refrigerated to 4 °C, and tested at 1 hour intervals after removing from the refrigerated environment. The indentation pilot

study confirmed the expected trend that as the tissue approached room temperature, a stiffness decay effect would be observed. While only shown on one trial, this type of experiment was repeated for the organs (kidney, liver, spleen) of n = 4 porcine animals ex-vivo.

After validating the device ex-vivo on a lab bench, we moved to test the device in-situ on a porcine carcass. Testing in-situ, we immediately struck an issue – indentation on the carcass yielded highly volatile results. There were a few factors that caused it, one of which was the peristalsis of the porcine intestines (still active post-mortem) introduced significant anatomical based noise in the data. The noise in Fig. 2.9 for the cold trials is acceptable because it can be filtered; but for the motion induced noise the signal to noise was too large and thus un-filterable. Compounding this issue, was the observation that our indentation platform was causing non-trivial displacements to the in-situ porcine organs due to a lack of a rigid support behind the organ. We attempted to mitigate this by placing a rigid support behind the tissue during the indentation, but the results still were not reliable and consistent enough for our purposes, nor was it practical for a minimally invasive in-vivo experiment.

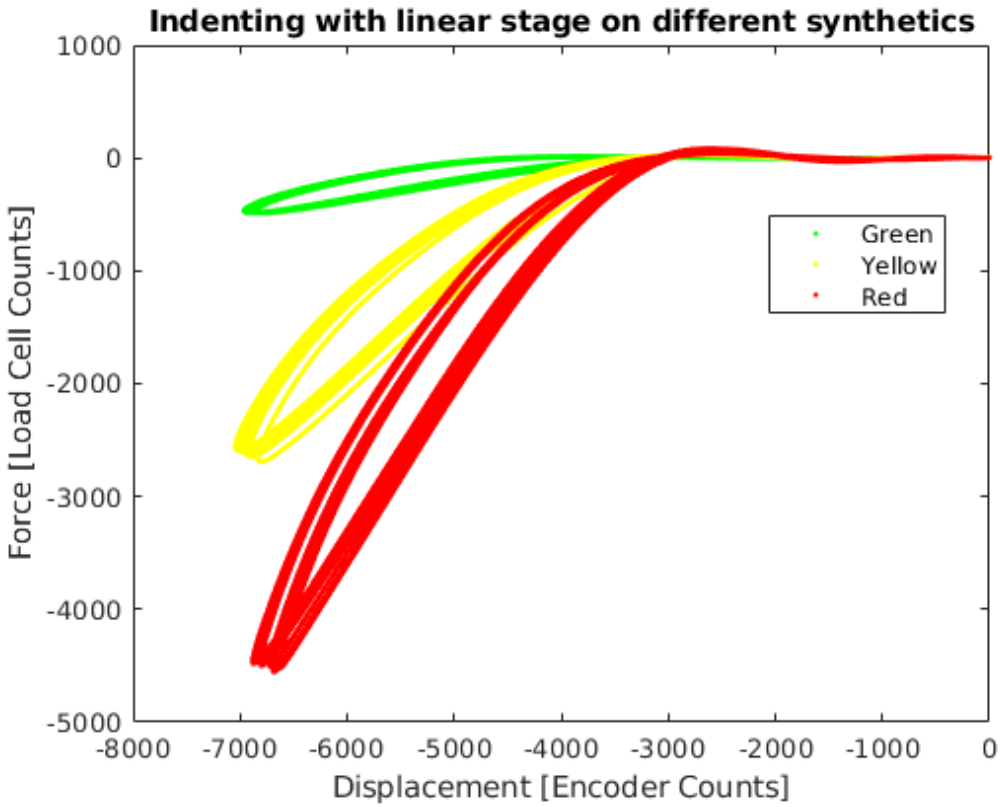

Figure 2.7: Uses pre-prototype indenter to test on various synthetic tissues. Color indicates relative stiffness – red > yellow > green. Each color was indented at 3 different thicknesses, the overlap of each curve within a material is representative of the geometry agnostic nature of indentation.

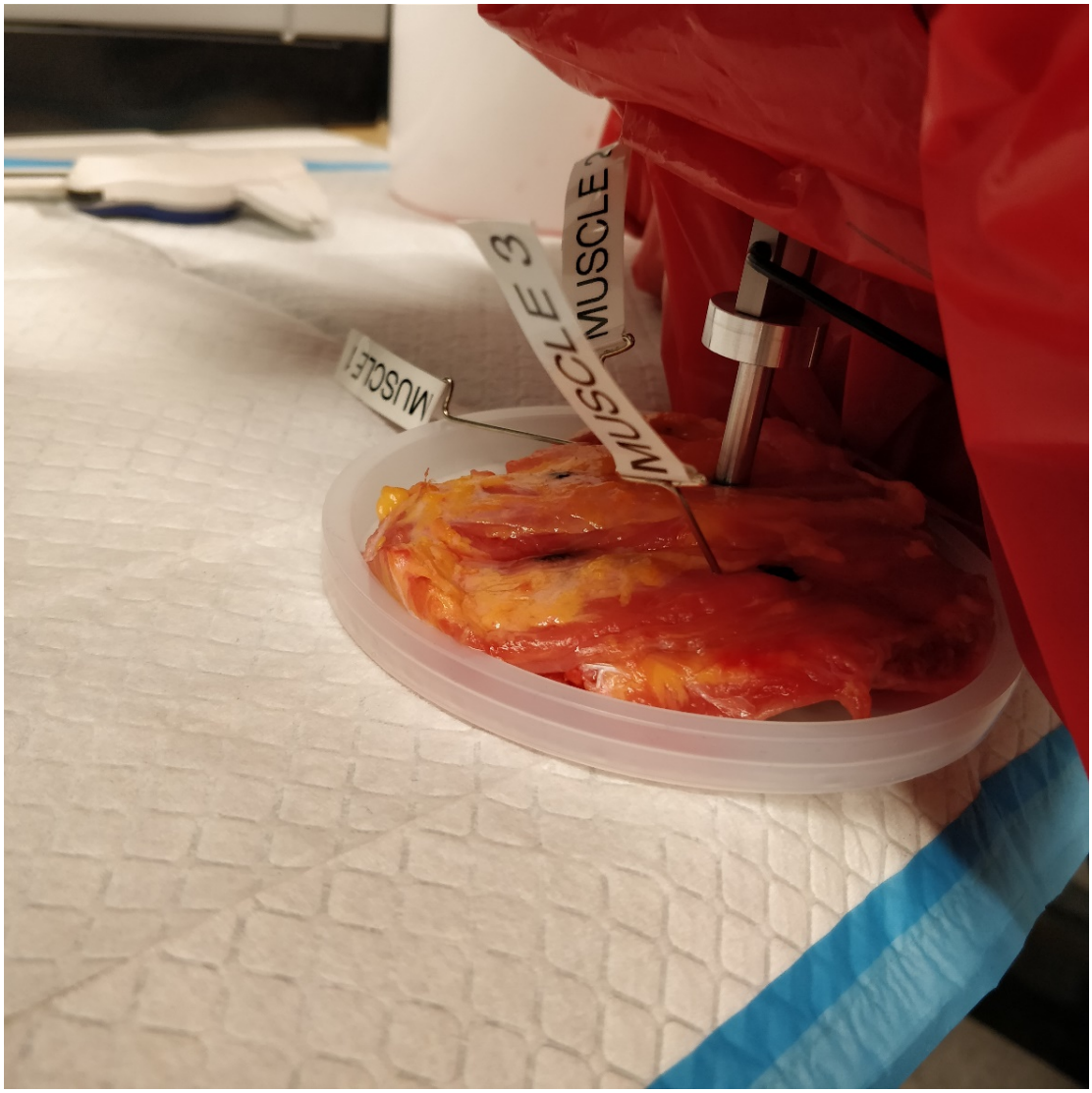

Figure 2.8: Photo illustrates indentation experiment of porcine muscle tissue.

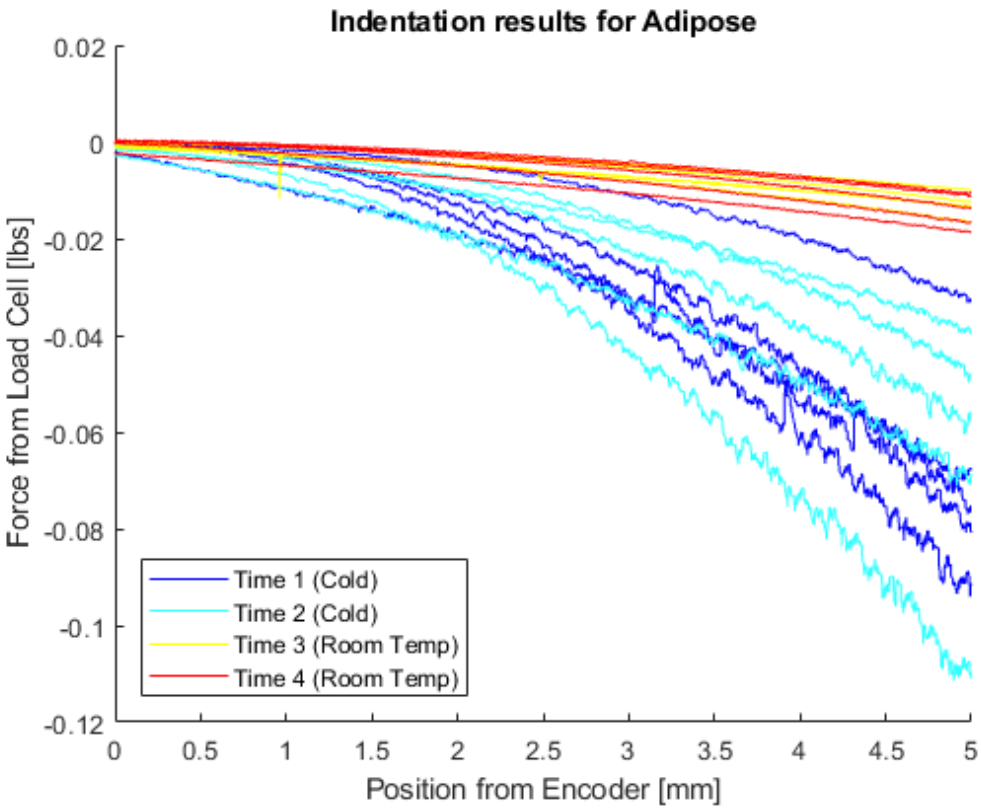

Figure 2.9: Results from indentation experiment on porcine adipose tissue. Tissue was tested under 4 conditions, 2 of them under room temperature, 2 of them at 4 °C. Time 1 represents tissue immediately removed from a fridge, Time 2 is one hour after Time 1, Time 3 is 3-4 hours after Time 2, and Time 4 is 1 hour after Time 3.

2.3 In-vivo Mechanical Grasping Device

Ultimately, these two platform designs failed to properly meet the deliverables of the project, requiring a fundamentally major design revision. The key lessons we learned was that the fundamental issue with the da Vinci grasper was the uncertainty introduced by the cable-pulley system, and how the cable tension dominates the mechanical response instead of the material-jaw interaction. Another way of phrasing this is that the lack of sensing at the jaw end effector, and being forced to predict end effector behavior using back end dynamics was not reliable for the accuracy and precision needed to distinguish in-vivo to ex-vivo mechanical responses. The inability to fixture and hold the organs consistently made indentation unacceptable for suitability in-vivo.

The next and final design, we sought to combine the benefits of each approach into one. The grasper had the primary advantage of being adept at experimentation in an in-vivo setting because it was explicitly designed for surgical interactions in the first place. An added benefit was that the dual jaws allowed for the tissue to be mutually anchored, obviating the issue we encountered with indentation. Indentation proved to be incredibly successful because of its ability to be effectively geometry independent, provided the location chosen was sufficiently "vast" and flat. The final design iteration captured the best of these two prototypes: a grasper with proper sensors at the end effector, utilizing indenter-like semi-spherical tips.

2.3.1 Hardware

A custom aluminum hand held grasping device, loosely intended to mimic a pair of surgical forceps, was instrumented with two 5 kg load cells (TAL220B, HT Sensor Technology) along each end, with 10 mm hemispherical attachments serving as the end effectors [Fig. 2.10, 2.11]. Hemispherical attachments were chosen because it allows the grasping experiment to be comparable to indentation of an infinite half-space under certain conditions. Each load cell was connected to a signal conditioner (IAA100, Futek Inc). The grasper jaw angle was measured using a quadrature rotary encoder with index pulse functionality (AMT102-V, CUI Inc) with a resolution of 0.7°. Both sets of instrumentation were connected to a NI PCIe 6320 DAQ card; data was acquired at 1 kHz using the NI-DAQMX C API on a Linux based PC. Data acquisition of force and

Figure 2.10: CAD render of In-vivo Mechanical Grasping Device instrumented with encoder and load cells.

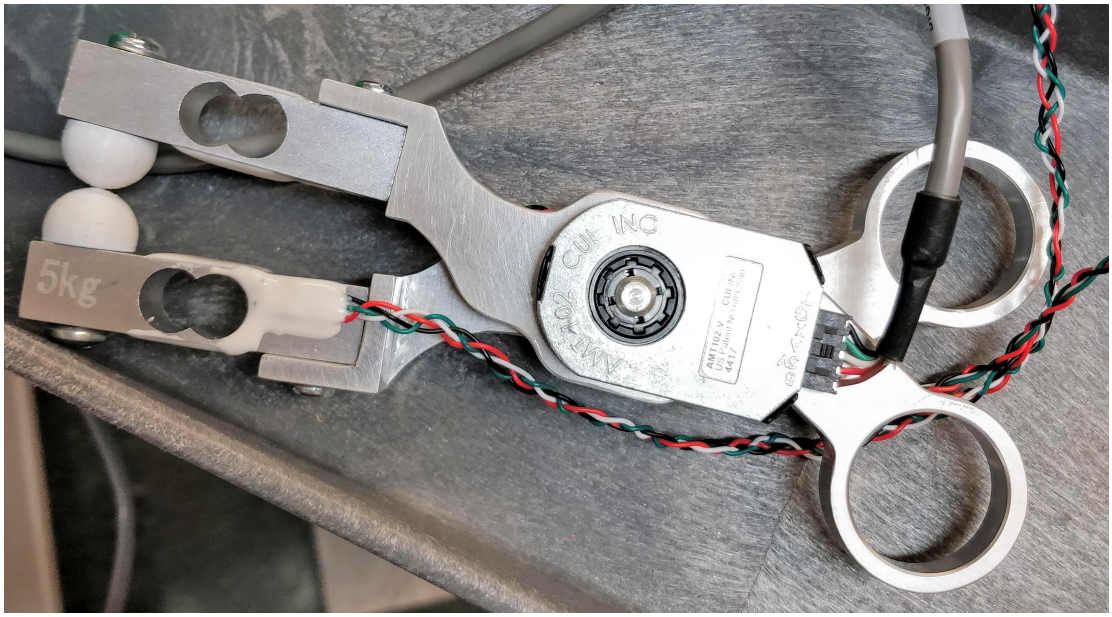

Figure 2.11: Photo of In-vivo Mechanical Grasping Device. The grasping end effector has spherical attachments, experimentally mimicking spherical indentation under certain conditions.

jaw angle was controlled and monitored via a custom GUI display which is described in the following section.

2.3.2 Software

Most of our lab's previous work in custom data acquisition systems revolved around Teensy microcontrollers and other small low voltage accessory electronics. Data from this ensemble was then transferred over serial using a USB cable. This is how the indenter was designed to function. One bothersome issue I have encountered with USB serial communication is that as you saturate the link bandwidth, the port(s) often start to lock up. I have experienced this in both Linux and Windows operating systems. A workaround I employed for the indenter was to instead send data using the HID protocol instead of serial. This increased the reliability of the data transmission at the expense of the transfer bandwidth (64 kB/s instead of 10 Mb/s).

In an effort to make the entire data acquisition pipeline more robust, and enable higher throughput for future projects that wish to use this platform, we moved the project to using National Instrument DAQ cards. NI provides a C based API to communicate with their various DAQ hardware. Instead of writing the data acquisition console in C, which would have been rather error prone due to the asynchronous nature of the hardware – I opted to write the underlying back end using Rust. Rust aims to be a comprehensive replacement to C, and while it is not 100% there yet, for 99% of use cases it delivers the revolution to programming that C once did for assembly programmers many years ago.

A Rust wrapper over the NI-DAQMX C API was created and used to communicate with the DAQ hardware. This backend was written using Rust's Futures, a model for asynchronous IO which mapped well onto the asynchronous nature of the NI-DAQMX library. This backend communicated onto a simple web application written in HTML/CSS (with theming provided by Bootstrap 4.0) which provided the front visual interface seen in Fig. 2.12. The advantage to all of this is that the data acquisition has become more robust, using industry standard NI DAQ hardware – allowing data collection rates to hit upwards of 100 kHz.

Figure 2.12: Screenshot of data collection GUI dubbed the "Scissors Console". Users can set the data filename and folder path. Buttons control when to start and stop data collection, as well as log clearing. A plot on the bottom of the screen displays the incoming data in real-time, allowing users to immediately be aware of data collection issues during the experiment.

Chapter 3

Methods

3.1 Experimental Design: in-vivo [Planned, Not Conducted]

The following section was written originally with the intention of including the in-vivo dataset in this thesis; experiments which at the time of publication, were not started nor completed. This section has been included without modification of tense – it is the authors intent that the reader interpret this section as how the Methods should read had the in-vivo experimentation been completed.

Porcine tissue experiments were conducted in close collaboration with the Visible Heart Lab from the University of Minnesota's Department of Surgery. All of the experimental protocols and setup were approved by the University of Minnesota's IACUC board, and by the USAMRMC ACURO committee. The in-vivo and ex-vivo mechanical characterization experiments were conducted on the liver and spleen of 5 adult pigs sourced from approved vendors by the US FDA. The animals were laid in the supine position and anesthetized intravenously by VHL personnel. Access to the liver was provided by a 3 in lateral incision immediately above the diaphragm region using electrocautery. The spleen was similarly accessible via a 2 in vertical incision on the animal's left side, starting just below the mid-line of the lateral incision. Incision size was minimized to balance the need for sufficient access to conduct the experiment, and the need to minimize animal bleeding. Organs were gently handled so as not to significantly alter their natural mechanical states, allowing the collected data to be as faithful as possible to their properties in-vivo, in-situ.

The target organs were tested under 5 experimental conditions [Table 3.2]. After the testing in-vivo (Condition 1) was completed, the organs were given 15 minutes to re-cooperate and return to their undisturbed mechanical states. During this time lab personnel prepared the animal for euthanization under an appropriate IACUC and ACURO approved protocol. Post euthanasia, the existing incisions in-vivo were enlarged to enable full access to the organs while remaining in-situ. Upon conclusion of testing for Condition 2, the organs were dissected and harvested, and transported to another site for further testing. During this time the organs' temperature typically decayed from physiological temperature to room temperature. We prioritized the immediacy of testing as soon as possible post-mortem to minimize tissue property decay, and hence the organs were not reheated in a water bath for Condition 3. Preparation for Condition 4 was conducted upon conclusion of Condition 3. This included dissecting the liver into its constituent lobes to facilitate easier reheating in a water bath, and storing each lobe/organ in a bag containing a 20 mL 1x PBS/Pen-Strep solution. The bagged organs were then stored for 18–36 hours (typically 24) in a refrigerator set at 4 °C. At the end of this duration and prior to testing for Condition 4, the organs were reheated to physiological temperature (37 °C) in a water bath for 2 hours. Following testing, the organs were frozen at -20 °C for 72–168 hours (typically 120) for the last round of experiments in Conditon 5.

On the morning of the experiment, the data collection system was setup on a mobile cart and the supplies for the experiment were restocked. The load cells were re-calibrated using an array of known masses, the signal conditioner re-tared, and our video equipment was checked for sufficient battery and storage capacity. The load cells were checked to have a zero load signal within ± 0.05 V, and the encoder was checked to ensure the index pulse was properly triggering and the values were within our expected ranges to ensure the bearing did not misalign or slip. Immediately prior to testing each organ, the grasping protocol was first performed on a silicone synthetic material as one final check to ensure the equipment was operating properly. A nitrile glove was affixed to the grasping device to protect the load cells from damage.

For each experimental condition, the test procedure was conducted by assigning each lab member a role. The roles are summarized in the Table 3.1. When all members were ready to begin a trial, the Grasping Tool Operator would begin by grasping 3 times

in-air to trigger the index pulse. Following this, 10 grasps were conducted on the target site on the organ at a rate of roughly 3 grasps per 5 seconds. This rate was enforced by having the Tool Operator grasp in synchrony with an audio recording at a similar beat frequency. Upon conclusion, the Tool Operator would note any observations to be recorded to the Study Coordinator, and next grasping site is identified. Criteria for acceptable grasping sites include: avoiding major blemishes, avoiding slippery regions, avoiding extraneous anatomy (i.e. gallbladder), remaining at least 1 cm away from the organ edge, and avoiding locations within 1 cm of other grasping sites. Effort was taken to ensure that a diversity of organ locations were tested in a randomized fashion. Condition 5 was an exception to this, in that locations that were identifiable as previous testing sites were specifically chosen. These steps were repeated a total of 10 times on the liver, and 7 on the spleen for each experimental condition. Trials that had significant tissue damage, slippage, and other anomalies were noted and not counted as successful. In each condition, the minimum acceptable number of successful trials was 7 for the liver, and 5 for the spleen.

Role	Responsibilities
Grasping Tool Operator	Performs experiment on tissue with device, marks tissue locations
Data Collection Monitor	Controls data collection on PC using GUI, monitors for sensor anomalies
Tissue Holder	Holds the tissue for the tool operator, helps select tissue locations
Study Coordinator	Ensures all members are adhering to study protocol

Table 3.1: Summarizes the various roles needed to perform the tissue experiments

Condition	Tissue State	Time After Death [hr]	*in/ex situ*	Temperature
1	*in-vivo*	N/A	*in-situ*	Body [37° C]
2	***ex-vivo***	0–1	*in-situ*	Body [37° C]
3	*ex-vivo*	1–2	***ex-situ***	**Room [23° C]**
4	***ex-vivo*, post refrigeration cycle**	18–36	*ex-situ*	Body [37° C]
5	***ex-vivo*, post freeze cycle**	72–168	*ex-situ*	Body [37° C]

Table 3.2: Table depicting the various experimental conditions. Bolded entries denote a change relative to the condition immediately above.

3.2 Data Analysis

The raw force and displacement vs time data was segmented to generate force-displacement plots. This segmentation was conducted by first linearly re-interpolating and synchronizing both time series to occur at the same time points. This is necessary because both datasets, while sampled at the same frequency, were not sampled at exactly the same time due to being on different timing subsystems within the NI DAQ card. The grasp segmentation was then performed on the time synchronized data. The first step was to level shift the forces recorded in the first two jaws, in effect taring the load cells in post. The next step converts the encoder counts into a real world jaw angle; this takes into account the radius of the jaws, the encoder index pulse and the encoder resolution. Grasps are segmented by 3 threshold criteria: minimum force, minimum rate of change in force, and minimum displacement. These thresholds were determined experimentally by trial and error, until all grasps were properly segmented and confirmed via manual inspection of the plots. Regions of data that did not meet these criteria were segmented out, and the remaining data was stitched together. Once stitched together, grasp displacements and normalized displacements could be calculated locally for each grasp.

After properly segmenting all the grasps, despite our best efforts a non-trivial percentage of them still possessed unique oddities that are not present in the bulk of the dataset. Experimentally it was determined that the following criteria of interest for each grasp was suitable for detecting anomalies that could be justifiably culled from the dataset. The points of interest included the maximum jaw force, maximum jaw displacement, initial tissue thickness, and goodness of fit (R^2) to an exponential. Each of these criteria were calculated for each segmented grasp. Within the bulk dataset of interest, grasps that possessed points of interest that were 3 median absolute deviations from the median were excluded from analysis on the basis that they were outliers. Before any comparisons were made on the fully processed grasp data, we noted that the tissue thickness was a confounding variable in the plots, thus the displacement was normalized in the subsequent analyses. When testing on synthetics, normalization of the displacement was sufficient to factor out the effects of differing thicknesses.

The force displacement data was analyzed using three different paradigms: under a

model free data driven context, using a traditional finite element modeling approach, and lastly a curve fitting approach inspiried by Rosen et al. In the model free method, for each condition and trial, we identified three pseudo-strain regimes which we refer to as the Low, Medium, and High (L-M-H) regions respectively and directly compared the force values. For liver this was chosen to be 0.1, 0.5 and 0.65 stretch ratio respectively, and 0.1, 0.5, and 0.95 for spleen. The intent of this analysis is to present a simple 1 dimensional snapshot of the tissue response at 3 different points along the curve. Under the curve fitting approach, the grasp force displacement curves were fit to a simple exponential model [Eq. (3.1)] where we take f to be the force, d_n to be the normalized displacement, and a b represent fit parameters. Here the product ab is interpreted as a "stiffness" in the sense that it is the derivative of a force-displacement relationship [Eq. (3.2)] – this notion is quite similar to that of a spring constant. The a term is interpreted as loosely being indicative of the toe region of the curve, while the b term of the exponential is considered as the term describing the strain hardening properties of the material.

$$f = a\left(e^{b\ d_n} - 1\right) \tag{3.1}$$

$$f' = ab\ e^{b\ d_n} \tag{3.2}$$

The naive approach to statistically analyze the data would be to do a series of Student's t-tests. This major pitfall with this approach is that with a multitude of conditions to compare between and multiple parameters to investigate, the issue of finding spurious correlations and false positives becomes almost certain. A more robust way to statistically analyze the various parameters generated by the 3 paradigms, is to use a 1 way ANOVA test to globally measure the means across all conditions. The issue with this approach is that it is an "all or nothing" type of test, it tells you if there is a difference but does not suggest which combinations of conditions are responsible. The solution to this problem involves some rather complex statistics, fortunately most computer analysis software packages provide access to these techniques by directly consuming the output of an ANOVA test. For the purposes of our analysis, we used MATLAB's `multcompare` with default settings to make a large number of statistical

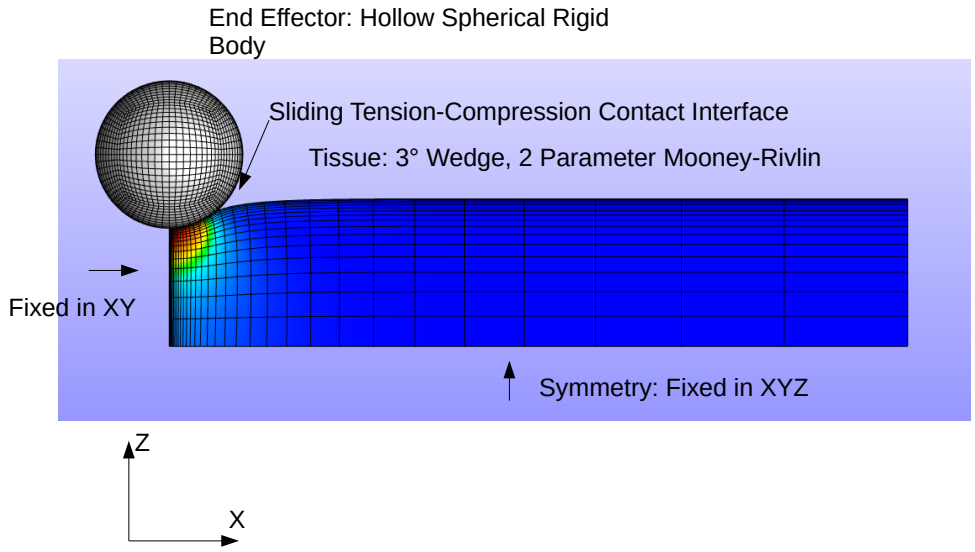

Figure 3.1: Side view of finite element model of the grasping experiment. End effector is modeled as a hollow spherical rigid body, tissue is modeled as a 3° wedge, with boundary conditions illustrated on the diagram.

comparisons while bounding our risk of making a false positive error.

3.3 Finite Element Modeling

Under the finite element modeling approach, FEBio 2.8 was used to model the grasping experiment. The tissue was modeled as a 2 parameter Mooney-Rivlin hyperelastic material with half the thickness of that measured in the experiment. A symmetry plane constraint was enforced as a zero displacment boundary on the back end of the tissue, simulating the full thickness. Only a 3° wedge of the tissue was modeled to take advantage of the radial symmetry of the problem. A native 2d model could not be used because Febio only supports 3d models, thus a wedge approximation was used. The axisymmetry is enforced by a tension-compression contact interface (penalty factor 10^4) with a rigid plane on one end of the wedge. The end effector is modeled as a perfectly rigid, hollow spherical body. FEBio's sliding compression contact model was used at the grasper-tissue interface also with a penalty factor of 10^4.

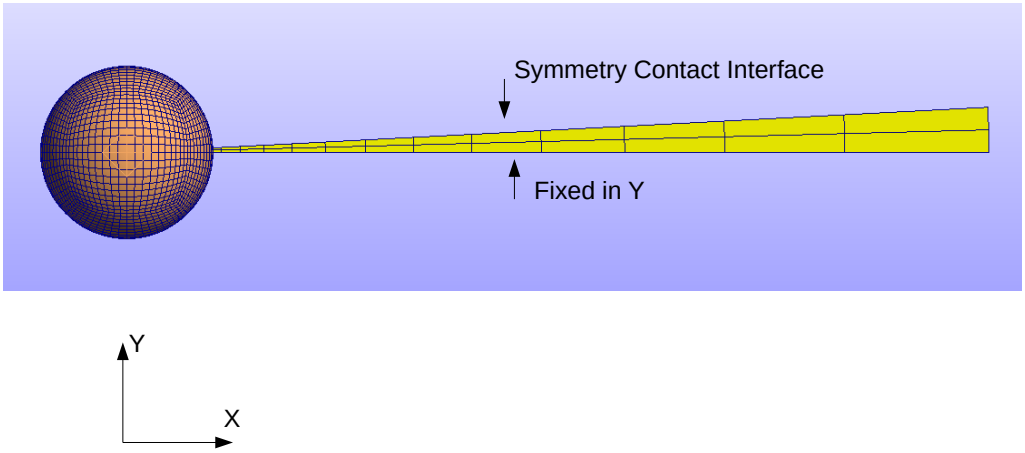

Figure 3.2: Top view of finite element model of grasping experiment. One side of the wedge has a fixed boundary condition preventing displacement along the y direction, the angled surface has a symmetry contact interface boundary condition.

The optimization module was used to take the forward finite element model with the experimental data to solve the inverse problem and determine the material parameters of the tissue. 10 representative data points from a grasp were used as the target response for the model to produce. The displacements from the experiment were prescribed in the model, and the FEBio optmization module iterated the material parameters until the error in experimental vs modeled response converged to a minimum. The material parameters for each grasp were then statistically compared in a similar fashion to the effective spring constants described above. A computer program was written to automate the process of generating model and optimization files that adapt the base files to match the grasp that was being simulated. This program would inject parameters such as the tissue thickness, grasp depth, and the 10 representative data points for the optimization to reproduce.

3.4 Preliminary Carcass Study

Since the in-vivo experimentation was not approved for scheduling in time for the publication of this thesis, to meet the research objective we instead perform a preliminary study on porcine carcasses. For this pilot run of data collection, n = 4 porcine specimens were tested with the final grasping prototype device in 3 of the 5 proposed conditions [Table 3.3]. The first pilot condition was conducted roughly 30 minutes post-euthanasia in the Visible Heart Lab, as soon as the VHL study was completed. The in-situ condition was conducted as proposed earlier in this chapter, the post refrigeration cycle condition (4) was skipped, and the post freeze-thaw condition was conducted instead within 24-72 hours (usually 24).

Condition	Tissue State	Time After Death [hr]	*in/ex situ*	Temperature
2	***ex-vivo***	0–1	*in-situ*	Body [37° C]
3	*ex-vivo*	1–2	***ex-situ***	**Room [23° C]**
5	***ex-vivo*, post freeze cycle**	24–72	*ex-situ*	Body [37° C]

Table 3.3: Table depicting the various experimental conditions used for the pilot study. Bolded entries denote a change relative to the condition immediately above. Note that for the pilot study only Conditions 2, 3, and 5 proposed in the Methods chapter were tested.

Chapter 4

Results and Discussion

As mentioned previously in this thesis, at the time of publication the in-vivo experimentation has not yet been conducted. The analysis presented below is on a pilot study on porcine carcasses.

The following subsections contain an array of figures which give the summary of the pilot data collected from the carcass experiments on both the liver and spleen. Figs. 4.1 to 4.6, and Figs. A.1 to A.12 are organized by two different strata. The data is first grouped into three categories based on the sub-grasps of interest – namely first grasps only, all grasps, and last grasps only where sub-grasp refers to the 10 grasps conducted on a particular region of tissue (within a trial). This was done to investigate the effect the sub-grasp had on the tissue, and whether the it was completely destructive or if the properties/response of the tissue remained largely the same. The next division is more mundane and is simply the tissue of interest – porcine liver or spleen. For the purposes of the subsequent analysis, only the first grasps of each trial are presented, with minimal commentary on the other grasps. The other figures can be found in the appendix.

Given a tissue type, and sub-grasp of interest, there are 3 plots presented. Fig. 4.1 shows an example of a 5x5 matrix of subplots showing a representative sampling of the force-displacement relationship, in this case for the first grasps on porcine liver. Fig. 4.2 is a set of box plots comparing the exponential fit parameters. The last figure within a cohort shows the Low Medium High analysis (L-M-H) at different force values. For liver, these stretch ratios (or normalized displacements) were chosen to be 0.1, 0.5, and 0.65 for the Low, Medium and High respectively. The values for the spleen were 0.1,

0.5 and 0.95. As a companion to each boxplot, a table summarizing the results of the ANOVA based multicomparison tests is provided.

To get a general overview of the dataset, the 5x5 matrix plots show a representative sampling of plots depicting the force and normalized displacement response of the tissues. The major take away is that following the outlier curve criteria outlined in the Methods chapter, almost all of the data fits incredibly well to a simple exponential. What is more subtle, is that the all grasps and the last grasps datasets have a few curves ($< 10\%$) that do not fit as well to an exponential – they have too shallow of a toe region and exhibit a sort of "lock out" effect that causes the force to rise too rapidly for a single term exponential to conform to. One example of this that is not quite pronounced is in Fig. A.1 on the bottom left corner – the orange fit just cannot quite wrap the elbow of the data in blue. More extreme examples are present in the appendix which also includes examples of curves that stay too shallow for an exponential to conform to. This observation, that grasps subsequent to the first one have a few outliers in shape, is what causes the oddities in the results for the datasets that include those grasps.

Out of the 3 different strata, the first one that presents interesting comparisons is the stark contrast in the dataset depending on which sub-grasps are included/excluded. The figures for the first grasp only dataset are among the cleanest and most well behaved in terms of outliers. Comparing the fit parameters for Fig. 4.2 and Fig. A.2 shows a significant difference in spread for the a term, and consequently the ab term. The first grasp only case has significantly tighter spread for the a term, whereas the spread is similar for both in the b term. That being said, there seems to be a sizable difference in the b coefficients when comparing the first grasp data and either of the other two conditions. If we interpret the a term as a numerical proxy describing the "initial state/condition" of the tissue, or in other words the toe region of the response – the variation in the toe region response is minimal for the first grasp, but is highly variable afterwards. The implication is that the crush injury inflicted by the grasp significantly influences its toe region behavior and thus the "response to initial contact" that is the most common sensation felt by a surgeon. In contrast, if we interpret the b term to represent the rate of stiffness change, a loose proxy for actual stiffness, it does not change as dramatically in value and especially not in spread following conditions common in tissue crush injury. In short, the first grasp is seen to significantly alter the tissue

response and it arguably makes the data from subsequent grasps not as relevant to simulation science since its not properly reflecting the native true response in a patient.

4.1 Preliminary Liver Data

Referencing Fig. 4.2 with its corresponding table of statistics, the liver data unanimously supports the conclusion that the in-situ to ex-situ transition causes a statistically significant change in properties. There was not a change from freezing the tissue according to the curve fit parameters. Dissecting the trends a little deeper, the reduction in the a coefficient over the testing life cycle suggests that the toe region of the curve is longer i.e. the tissue is less stiff at lower strains. However, this is contrasted by a small relative increase in the b coefficient which loosely characterizes the strain hardening properties of the material. The combined effect of the two, by taking the product, seems to suggest that the overall effect is a global reduction in stiffness – at least in the ranges of strains in our experiment. The plot showing the results from the more observational approach [Fig. 4.3], by looking at the forces at various strains seems to be inconclusive. The forces at the low and high strains indicate no significant change between conditions. However, the interesting result is that for medium strains, freezing the tissue seems to have a significant effect on the tissue.

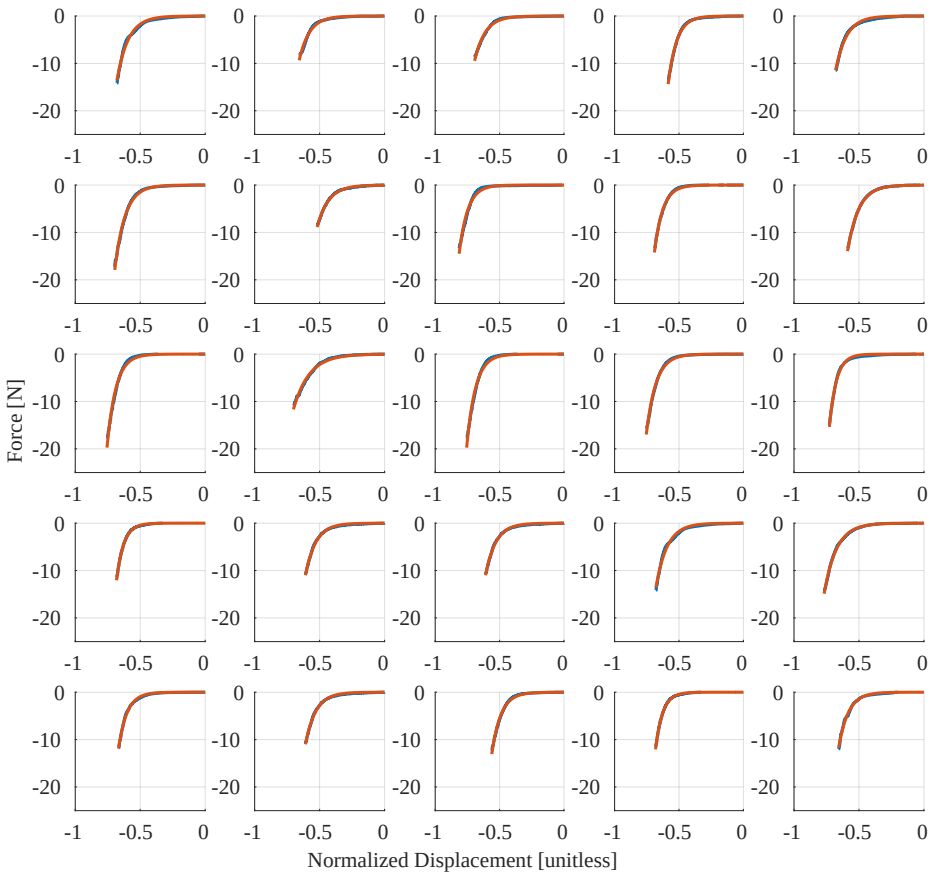

Figure 4.1: 5x5 matrix plot of sample grasps on porcine liver tissue. The blue curves represent the actual data, and the orange curve represents the exponential fit.

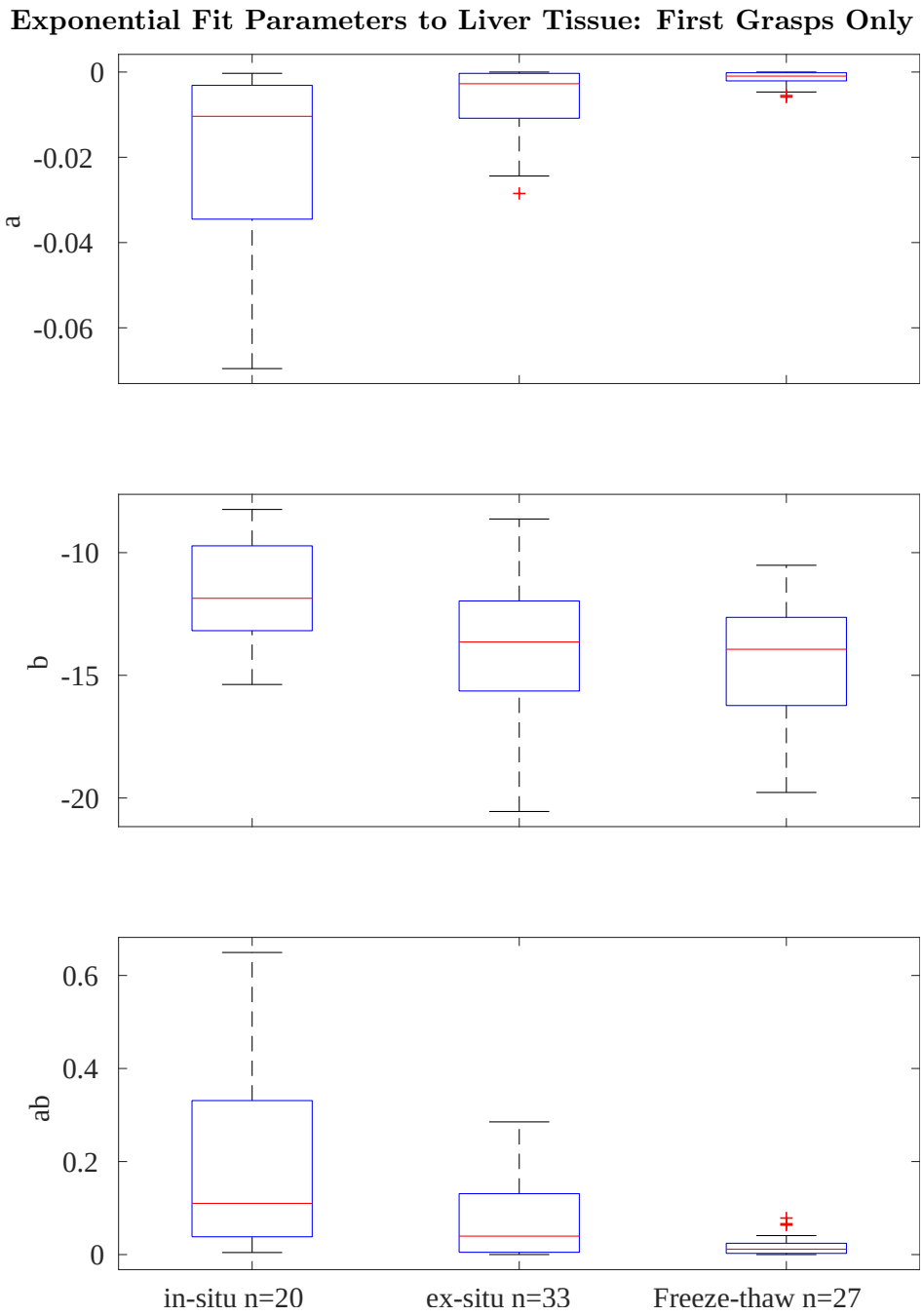

Figure 4.2: Box plots illustrating fit parameters for a single term exponential over grasps on porcine liver tissue.

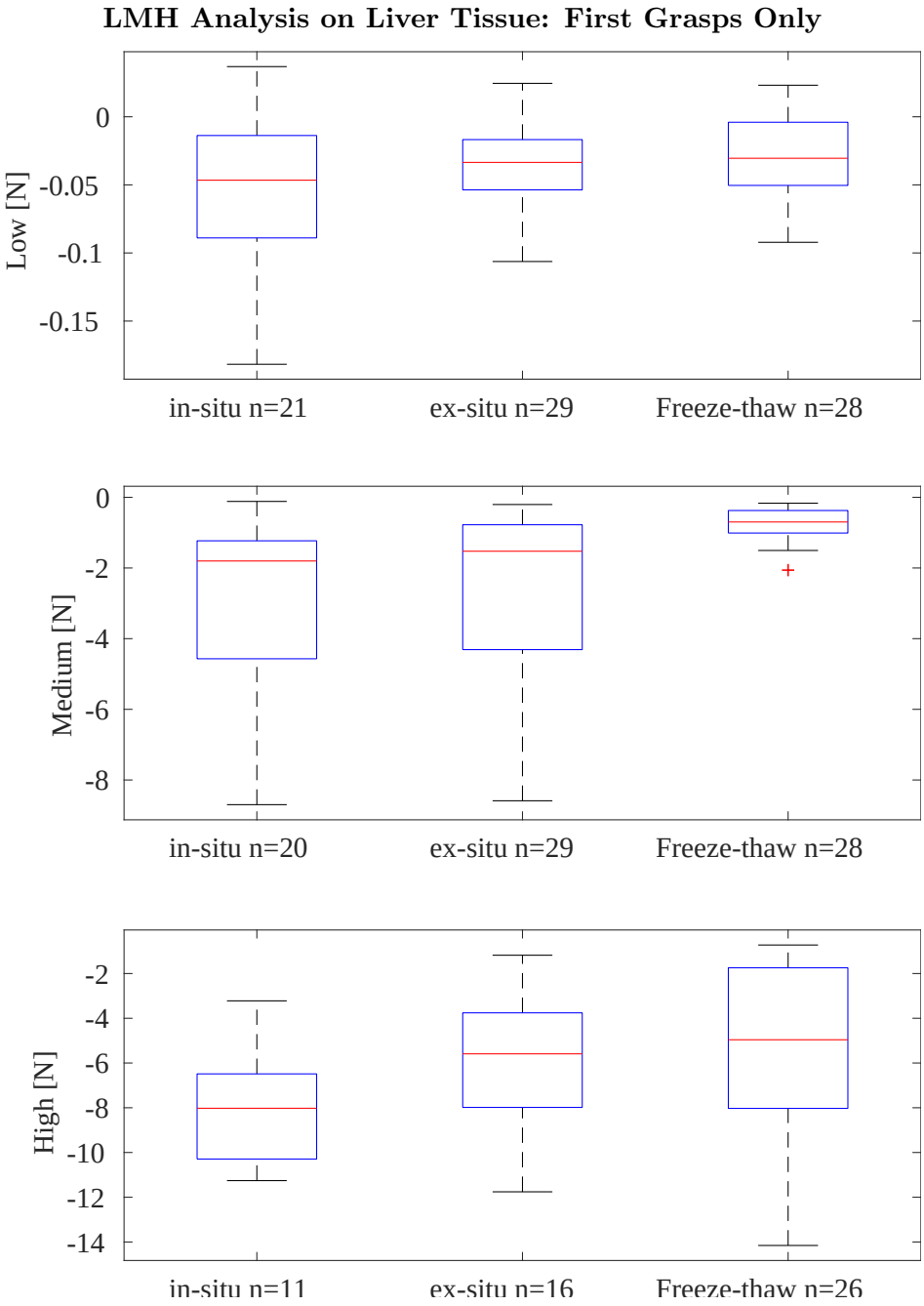

Figure 4.3: Box plots illustrating the "Low Medium High" (LMH) analysis of grasp data from porcine liver tissue. These were chosen to be 0.1, 0.5 and 0.65 for the liver, respectively.

Condition A	Condition B	$\mu_a - \mu_b$ Lower Bound	$\mu_a - \mu_b$	$\mu_a - \mu_b$ Upper Bound	p-value
a					
b					
ab					
in-situ	ex-situ	-0.0227	-0.0141	-0.00549	5.6e-4
in-situ	freeze-thaw	-0.0283	-0.0193	-0.0104	5.46e-6
ex-situ	freeze-thaw	-0.0131	-0.00525	0.00262	0.254
in-situ	ex-situ	0.53	2.2	3.9	6.7e-3
in-situ	freeze-thaw	0.86	2.6	4.4	1.9e-3
ex-situ	freeze-thaw	-1.2	0.4	1.9	0.81
in-situ	ex-situ	0.048	0.13	0.21	8.8e-4
in-situ	freeze-thaw	0.1	0.19	0.28	3.8e-6
ex-situ	freeze-thaw	-0.017	0.058	0.13	0.16

Table 4.1: Statistics corresponding to Fig. 4.2. Each sub-divided row of the table corresponds to each row of boxplots in Fig. 4.2. All p-values shown take into account the use of multiple comparisons – see MATLAB R2019a `multcompare`.

Condition A	Condition B	$\mu_a - \mu_b$ Lower Bound	$\mu_a - \mu_b$	$\mu_a - \mu_b$ Upper Bound	p-value
Low					
Medium					
High					
in-situ	ex-situ	-0.041	-0.015	0.012	0.39
in-situ	freeze-thaw	-0.048	-0.021	6.0e-3	0.16
ex-situ	freeze-thaw	-0.031	-6.1e-3	0.018	0.82
in-situ	ex-situ	-1.9	-0.44	0.99	0.74
in-situ	freeze-thaw	-3.8	-2.4	-0.91	5.9e-4
ex-situ	freeze-thaw	-3.2	-1.9	-0.61	2.2e-3
in-situ	ex-situ	-5.3	-2.1	1.1	0.26
in-situ	freeze-thaw	-5.3	-2.4	0.57	0.14
ex-situ	freeze-thaw	-2.9	-0.26	2.3	0.97

Table 4.2: Statistics corresponding to Fig. 4.3. Each sub-divided row of the table corresponds to each row of boxplots in Fig. 4.3. All p-values shown take into account the use of multiple comparisons – see MATLAB R2019a `multcompare`.

4.2 Preliminary Spleen Data

The spleen suggests similar conclusions to that of the liver. Fig. 4.5 for both the a and ab coefficients agree with the liver data and implicate a significant change in the move from in the carcass to the lab bench. Oddly, the b coefficient sees a significant bump from in-situ to ex-situ, but the change is reverted after freezing. The LMH results for the spleen differ a bit from the liver in that there are a lot more significant changes detected. The same oddity in the b coefficient for the spleen is observed for the low strain forces, a significant change after dissection but it is reverted after freezing. The medium strain forces make the common implication that dissection changes the tissue, but not freezing. And lastly, the high strain forces contrast this by saying the opposite – freezing is responsible for changing the properties, but dissection. Overall the results for the observational approach for the spleen are rather conflicting. The curve fit results are consistent with the liver results however.

Condition A	Condition B	$\mu_a - \mu_b$ Lower Bound	$\mu_a - \mu_b$	$\mu_a - \mu_b$ Upper Bound	p-value
	a				
	b				
	ab				
in-situ	ex-situ	-0.079	-0.049	-0.019	5.4e-4
in-situ	freeze-thaw	-0.081	-0.052	-0.024	1.2e-4
ex-situ	freeze-thaw	-0.03	-3.3e-3	0.024	0.95
in-situ	ex-situ	0.15	1.6	3.1	0.027
in-situ	freeze-thaw	-0.091	1.3	2.7	0.071
ex-situ	freeze-thaw	-1.6	-0.3	1.1	0.85
in-situ	ex-situ	0.08	0.2	0.33	6.1e-4
in-situ	freeze-thaw	0.11	0.23	0.34	7.8e-5
ex-situ	freeze-thaw	-0.092	0.022	0.14	0.89

Table 4.3: Statistics corresponding to Fig. 4.5. Each sub-divided row of the table corresponds to each row of boxplots in Fig. 4.5. All p-values shown take into account the use of multiple comparisons – see MATLAB R2019a `multcompare`.

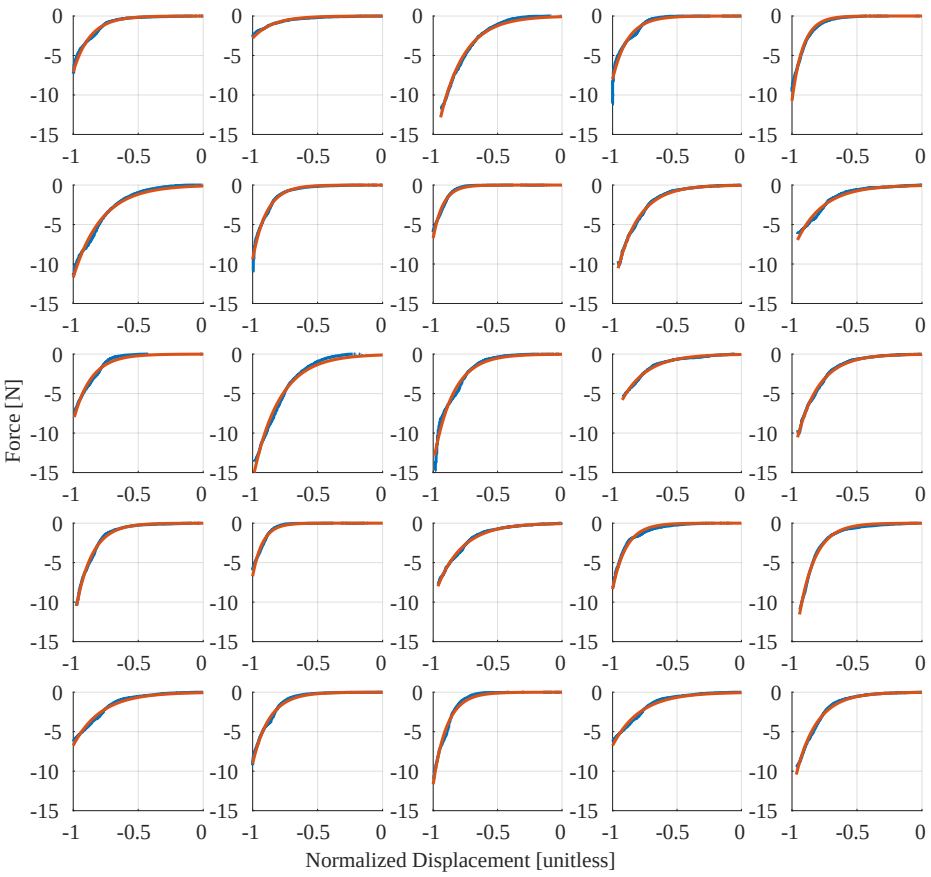

Figure 4.4: 5x5 matrix plot of sample grasps on porcine spleen tissue. The blue curves represent the actual data, and the orange curve represents the exponential fit.

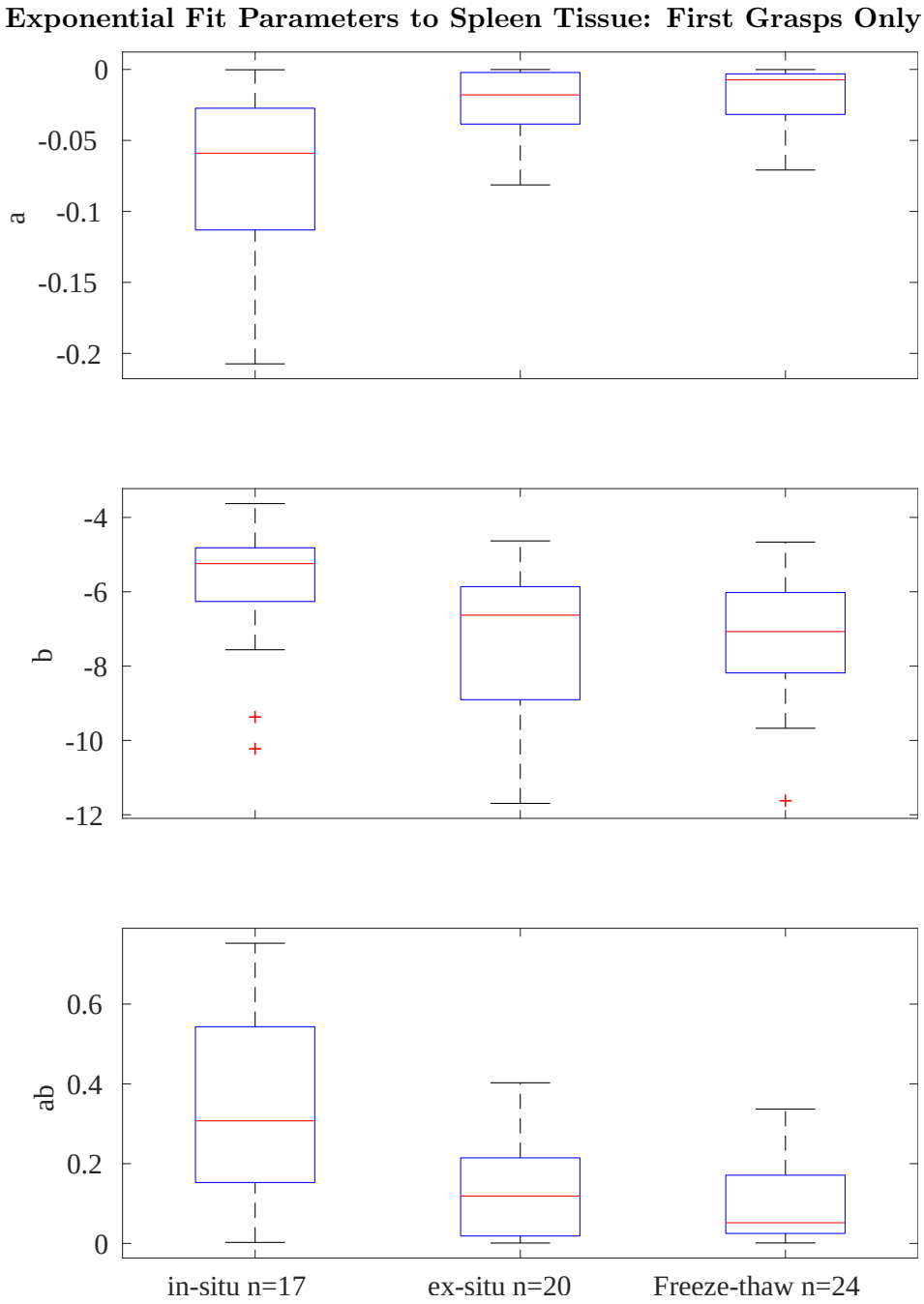

Figure 4.5: Box plots illustrating fit parameters for a single term exponential over grasps on porcine spleen tissue.

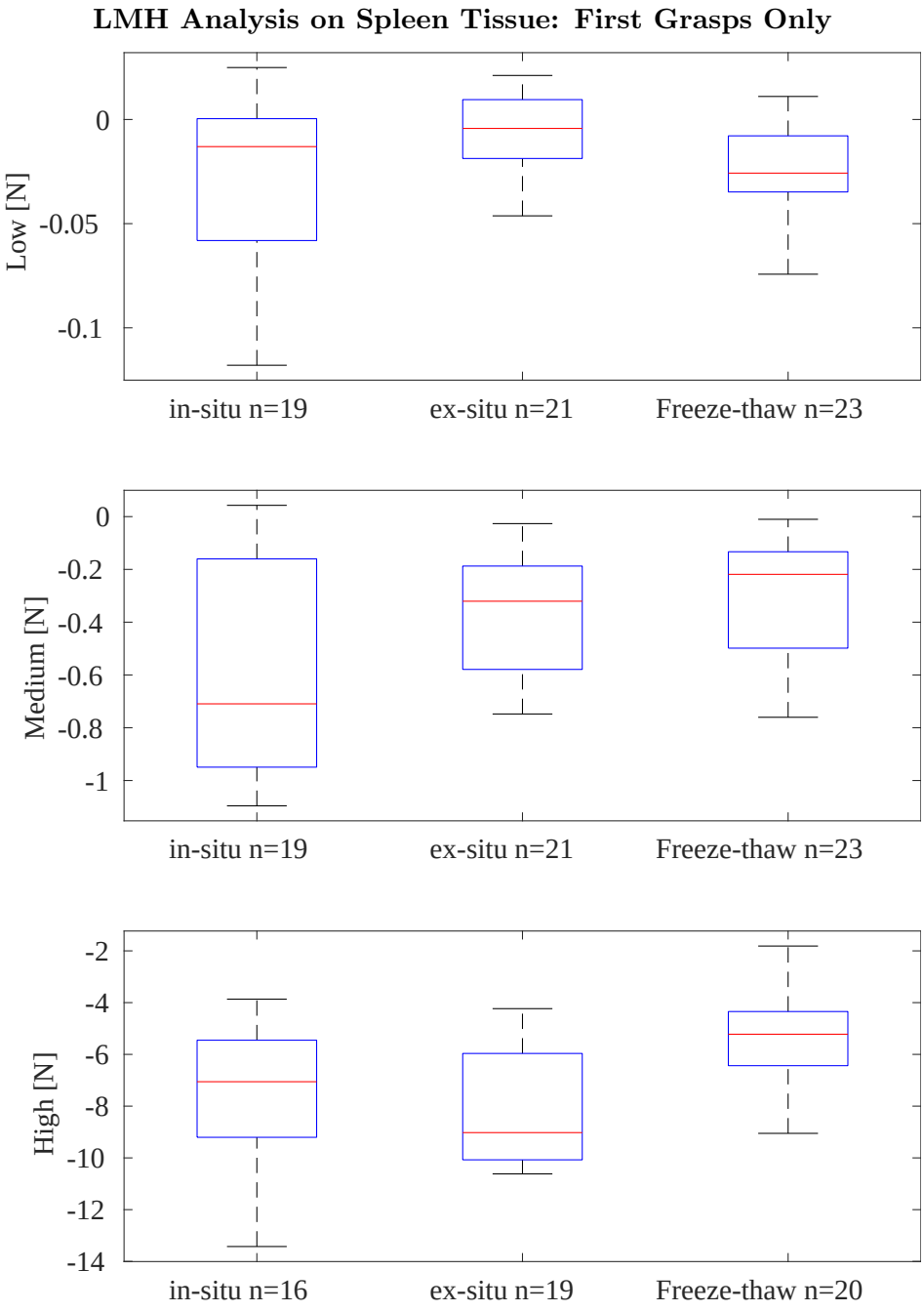

Figure 4.6: Box plots illustrating the "Low Medium High" (LMH) analysis of grasp data from porcine spleen tissue. These were chosen to be 0.1, 0.5, and 0.95 for the spleen, respectively.

Condition A	Condition B	$\mu_a - \mu_b$ Lower Bound	$\mu_a - \mu_b$	$\mu_a - \mu_b$ Upper Bound	p-value
Low					
in-situ	ex-situ	-0.045	-0.024	-3.1e-3	0.021
in-situ	freeze-thaw	-0.025	-5.1e-3	0.015	0.82
ex-situ	freeze-thaw	-1.1e-3	0.019	0.039	0.067
Medium					
in-situ	ex-situ	-0.44	-0.22	-5.0e-3	0.044
in-situ	freeze-thaw	-0.52	-0.3	-0.085	3.9e-3
ex-situ	freeze-thaw	-0.28	-0.075	0.13	0.66
High					
in-situ	ex-situ	-1.2	0.67	2.5	0.66
in-situ	freeze-thaw	-3.8	-1.9	-0.12	0.034
ex-situ	freeze-thaw	-4.4	-2.6	-0.87	2.0e-3

Table 4.4: Statistics corresponding to Fig. 4.6. Each sub-divided row of the table corresponds to each row of boxplots in Fig. 4.6. All p-values shown take into account the use of multiple comparisons – see MATLAB R2019a `multcompare`.

Chapter 5

Case Study: Urethral Catheterization

Note that much of this chapter is duplicated verbatim from the thesis author's abstract submission to the 2019 Design of Medical Devices Conference in Minneapolis Minnesota [18]. Additionally, this chapter also includes the author's abstract submission to the Engineering in Urology Society 2019 annual meeting. Both conference abstracts were presented by the author at their respective conferences. The last section ends with a brief discussion of some of the key results from a cadaver study that were not included in both conference abstracts.

5.1 Abstract

Catheter associated urinary tract infections (CAUTI) are among the most common nonpayment hospital acquired conditions. Inexperienced health care providers placing indwelling urinary catheters are associated with an increased risk of CAUTI. The creation of high-fidelity simulators may reduce CAUTI risk during critical early learning. As a first step toward the creation of accurate simulators our group set out to characterize the mechanical aspects of urethral catheterization. This work presents an inexpensive, yet practical means of acquiring motion and force data from urethral catheter insertion procedures using OpenCV ArUco markers. Evaluation of the video system's accuracy was done to understand the performance characteristics within the

boundaries of the procedure's target workspace. The tracking accuracy was validated to be roughly ± 3 mm in the plane of the camera, and ± 10 - 25 mm along its axis depending on the distance. Feasibility of using this platform in a clinically relevant setting was demonstrated by capturing the force and motion data when performing urinary catheterization on cadaveric donors (N=2).

5.2 Introduction

Catheter associated urinary tract infections (CAUTI) are the most commonly reported hospital acquired infection. CAUTI arise secondary to indwelling urinary catheter placement and cause increased hospital cost and patient morbidity [6]. While a great deal is known about patient and environmental factors that contribute to an increased CAUTI risk, only recently have studies began assessing providers who are placing indwelling catheters. Most notably, inexperienced health care providers placing indwelling urinary catheters are associated with a 4-fold increased risk of CAUTI [20]. One potential avenue to reduce CAUTI rates is to provide proper instruction, objective assessment, and accurate simulation during early clinical training or remedial testing.

Realistic simulators may better facilitate skill transfer into practice settings but this requires accurate knowledge of the mechanical responses of tissues to clinician motions such as friction force. This should span both typical and atypical anatomy as well as tissue responses resulting from proper motions and improper motions that lead to injury or potentially CAUTI's. Urinary insertion force has been subjectively self-reported by healthcare providers after completing a procedure [2]. To our knowledge, no research that has investigated the mechanics of urinary catheter insertion objectively and there is no readily-available device to measure required forces and motions. The objective of this work is to i) introduce a system to practically capture motion and force of typical urinary catheterizations, ii) determine the accuracy of this inexpensive motion capture method, and iii) demonstrate feasibility of clinically meaningful data acquisition on cadaveric donors.

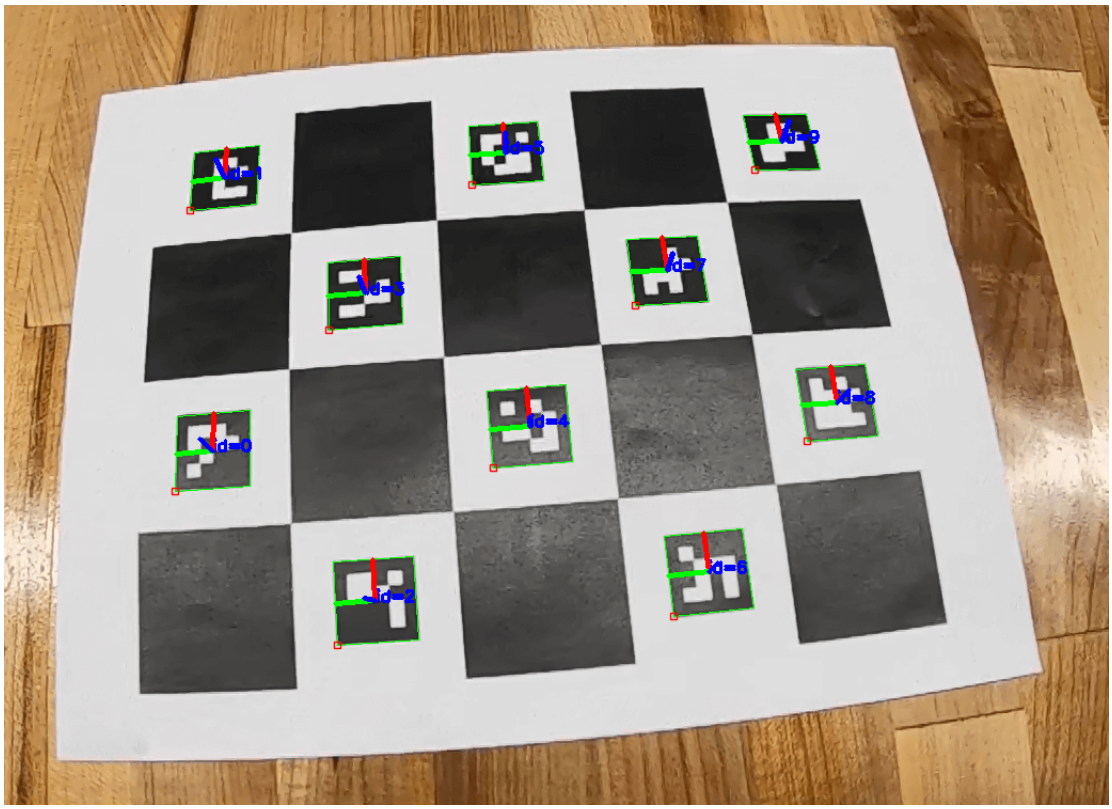

Figure 5.1: Example pose estimation (colored triads) extracted using OpenCV ArUco markers (8.5” x 11” standard U.S. paper size)

5.3 Methods

The mechanical characteristics tracking platform in this work leverages our prior work [9] which describes a catheter insertion force assessment tool. In short, this inexpensive device is comprised of a 3D-printed handle instrumented with two 780 g load cells (Phidgets Inc., Calgary AB, Canada) and two HX711 load cell amplifiers (SparkFun Electronics, Inc., Niwot, CO) to measure the insertion force. A Teensy 3.2 microcontroller (PJRC, Sherwood OR, USA), and bluetooth modem (SparkFun Electronics, Inc., Niwot, CO) served as a means to communicate data back to the host PC.

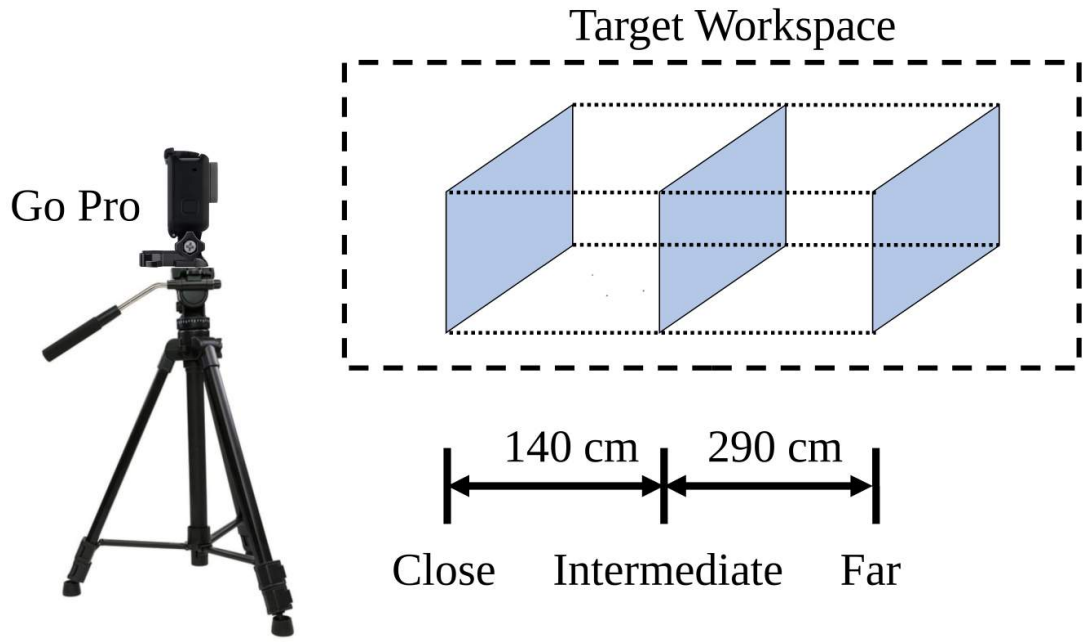

Figure 5.2: Experimental setup for measuring ArUco motion capture accuracy within target workspace of typical catheter insertion motions. Three regions: close, intermediate, and far are shown with known displacements. Intermediate represents approximate center plane of workspace in which majority of motions are expected to occur. The distance from the camera to the target workspace is approximately 270 mm

ArUco markers [5] were used to measure the 3 dimensional motion of the operator during the procedure with the Open Source Computer Vision Library (OpenCV) [16]. Video capture of the markers was facilitated by a GoPro Hero7 Black camera (GoPro Inc., San Mateo, CA) set to record 1080p footage at 240 FPS (1920x1080 pixels used in

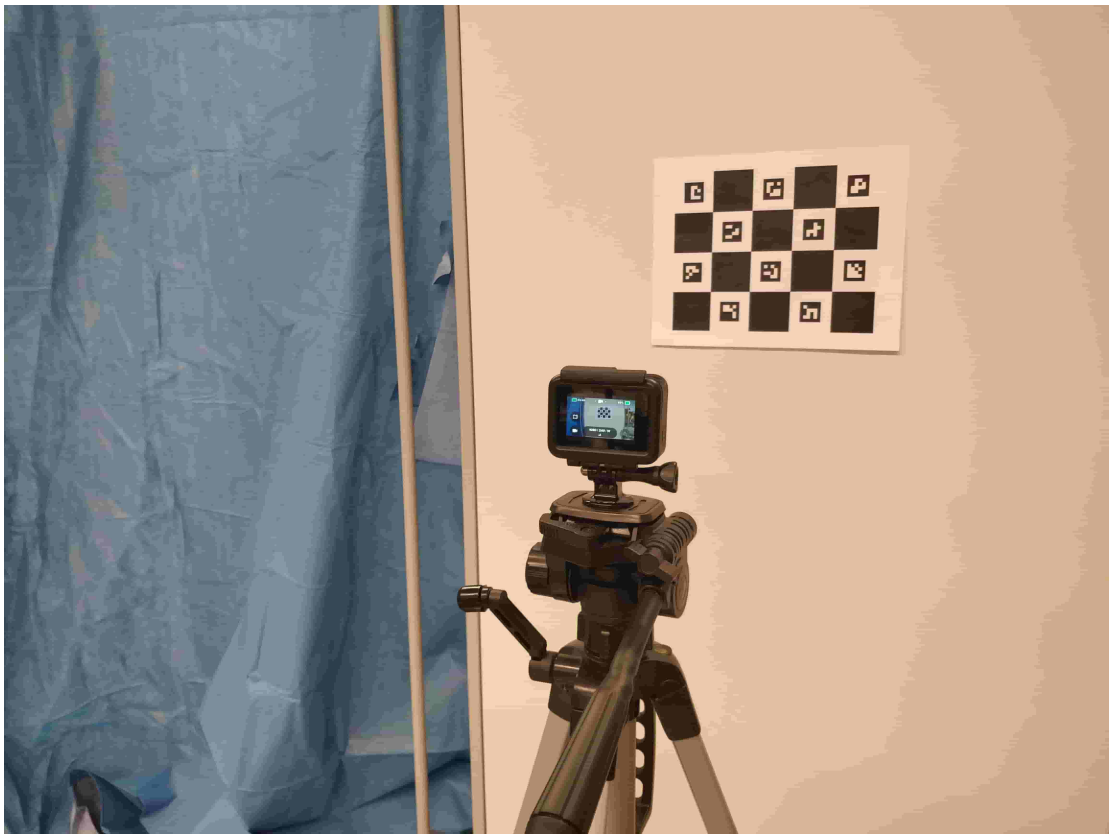

Figure 5.3: Photo of experimental setup in intermediate configuration

post-processing herein). The procedure in the ArUco library documentation was used to calibrate our camera and obtain intrinsic and distortion parameters [4].

The accuracy of the ArUco markers and video system was assessed in the a target workspace enclosing typical hand motion for urinary catheter insertion [Fig. 5.2, 5.3]. The "closest" configuration was roughly 270 mm away from the camera, and the displacement between the two successive configurations were known to be 140 and 290 mm respectively. At each configuration, the camera was set to record an array of ArUco markers as in Figure 5.1 for 3 - 5 seconds. The videos were then processed by OpenCV routines and the ArUco library, and the position data imported into MATLAB.

At each frame, the centroid of all the detected ArUco markers was computed which served as a reference point. The ground truth positions in the plane of the paper (hereby referred to as the XY plane) were measured via a caliper and compared to the output of the computer vision algorithm. For details on the underlying ArUco detection and tracking algorithms see [5].

To validate our device and tracking system for feasibility in a clinically relevant setting, procedure data was collected on two non-fixed male human cadevers by coauthor MT. Access to cadavers was granted through the University of Minnesota's Anatomy Bequest Whole Body Donation Program. The catheter insertion force assessment tool was used to place both a Foley, and Coude urinary catheter while subject to computer vision tracking [Fig. 5.4].

5.4 Results and Discussion

The ArUco computer vision algorithms for marker tracking are accurate, simple, and inexpensive to implement. In the XY plane, we observed a typical RMS error of 3 mm [Fig. 5.5]. In the z-axis (along the axis of the camera), larger errors were recorded – on the order of 10 - 25 mm depending on the distance away [Fig. 5.6]. Larger errors along the axis of a camera relative to in-plane errors are a well understood limitation in computer vision, reflected in the results presented here. Additionally, as expected there is a trend between increasing distance, and increasing error across both in-plane and out of plane measurements. Increasing distance between the camera and the target leads to a lower resolution capture of the marker, which leads to jitter in the detected

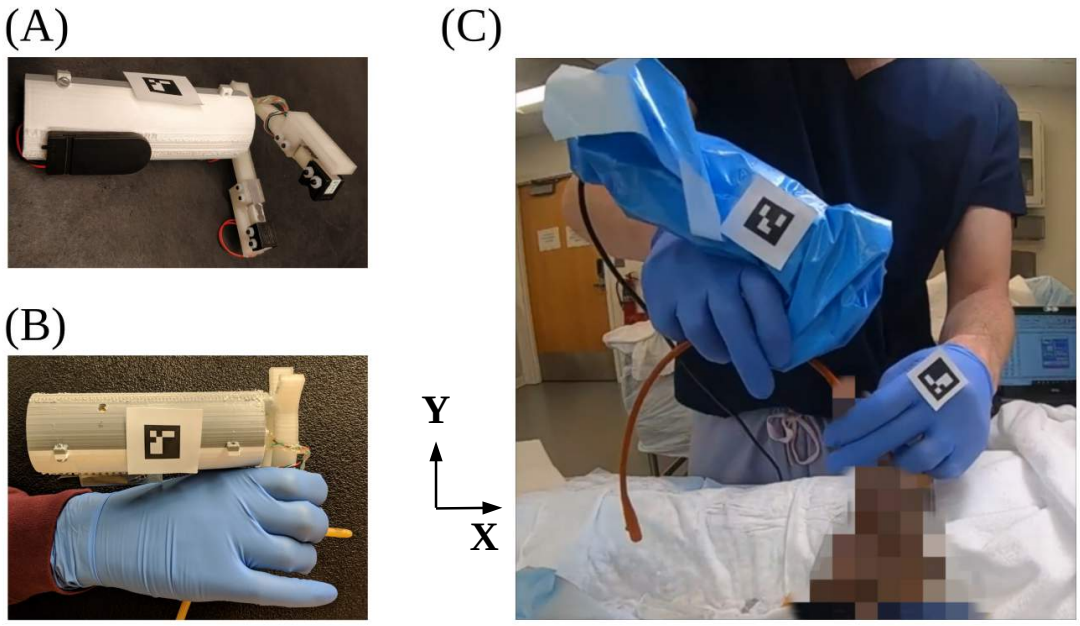

Figure 5.4: A, B) Photo of catheter insertion force assessment tool. C) Performing catheterization on unfixed cadaveric donor with device and tracking platform

output [5.10].

In the context of our application, urinary catheter insertion, the device primarily moves along a single plane. Thus proper camera positioning can mitigate the accuracy penalty incurred by motion in the z-axis. This affords us millimeter level accuracy when tracking motion during catheterizations. Admittedly, compared to the state of the art, EM based tracking, our computer vision based approach cannot deliver its sub-millimeter level accuracy. The strength of this work instead lies in its low cost and simplicity; anyone with a camera and inkjet printer can acquire catheter motion trajectories.

During the cadaver study, it was found that typical maximal urinary insertion forces were about 3 - 6 Newtons. The greater forces were often observed at the end of a "push-event" during insertion. The average speed of the catheter was 6 cm/s during the procedure. To better quantify the friction force during the insertion motion, the relationship between insertion force and velocity will be further examined in future work.

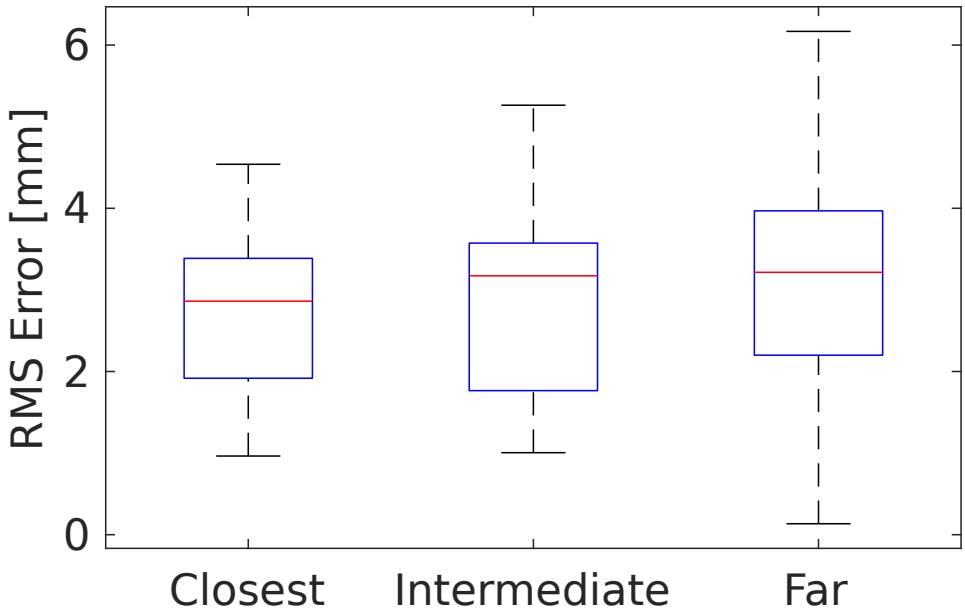

Figure 5.5: Root mean squared error in the xy plane from tracking experiment in all 3 configurations

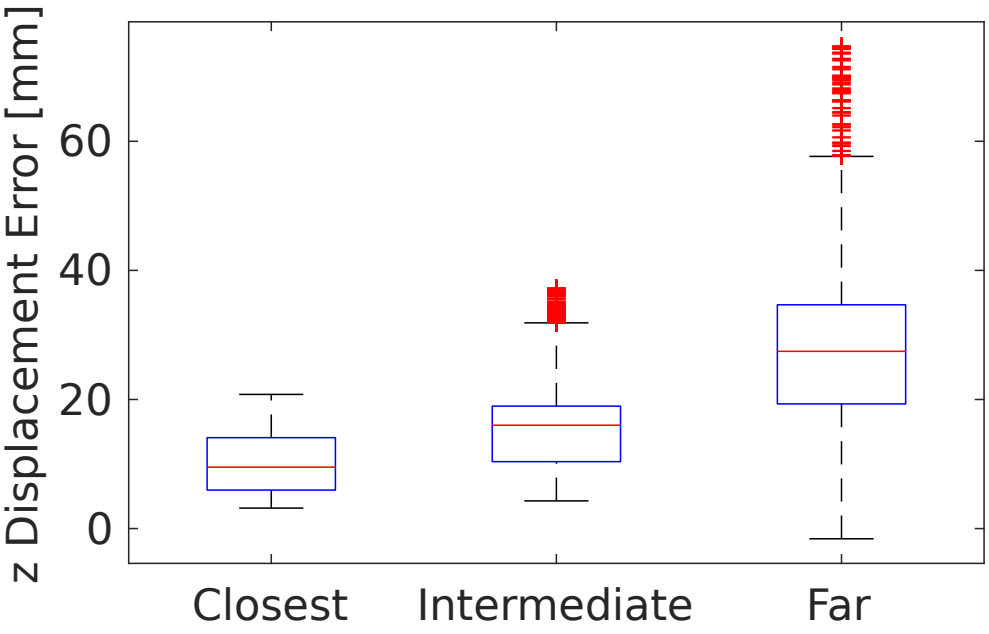

Figure 5.6: Z displacement error from tracking experiment in all 3 configurations

Understanding the mechanical factors in urinary catheterization, such as the urethral-catheter friction are the first step in acquiring data to better inform the development of next generation simulators.

5.5 Conclusion

This work demonstrates successful, practical motion and insertion force collection on urinary catheter placement in clinically realistic settings. Future work will seek in-vivo data from consenting patients.

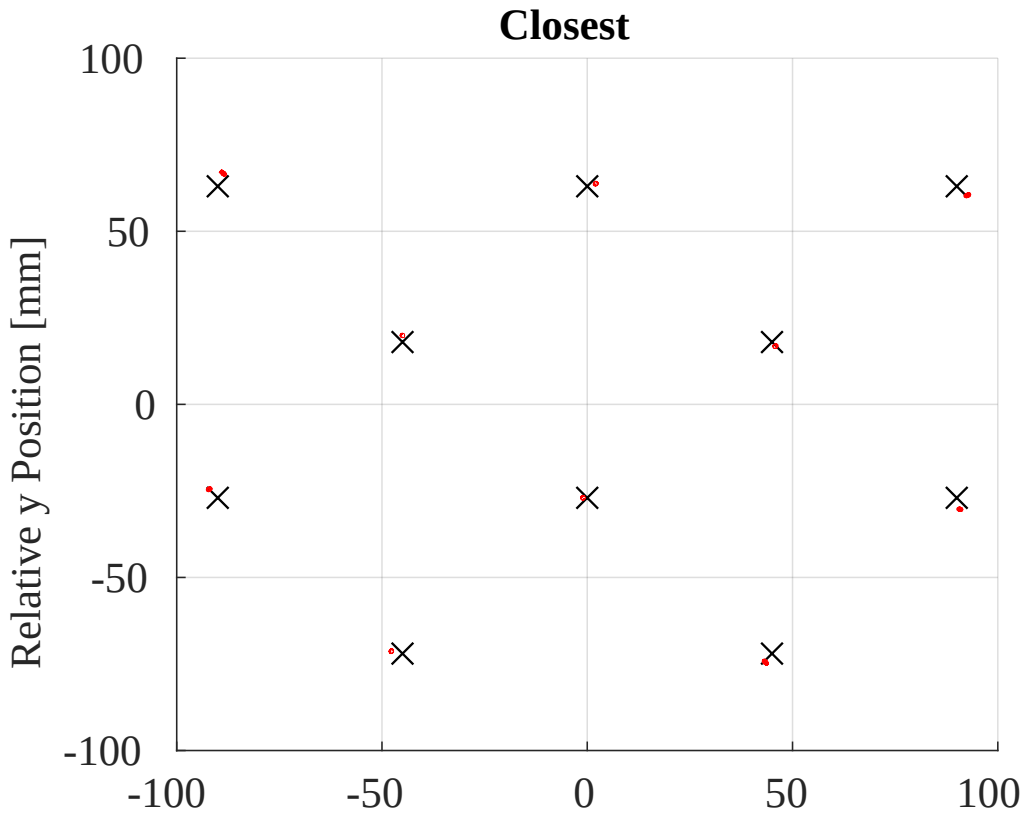

Figure 5.7: Depicts the relative accuracy in the XY plane relative to the ArUco grid. The ground truth (X) is compared with the measured output from the computer vision algorithm. This is shown for the closest configuration.

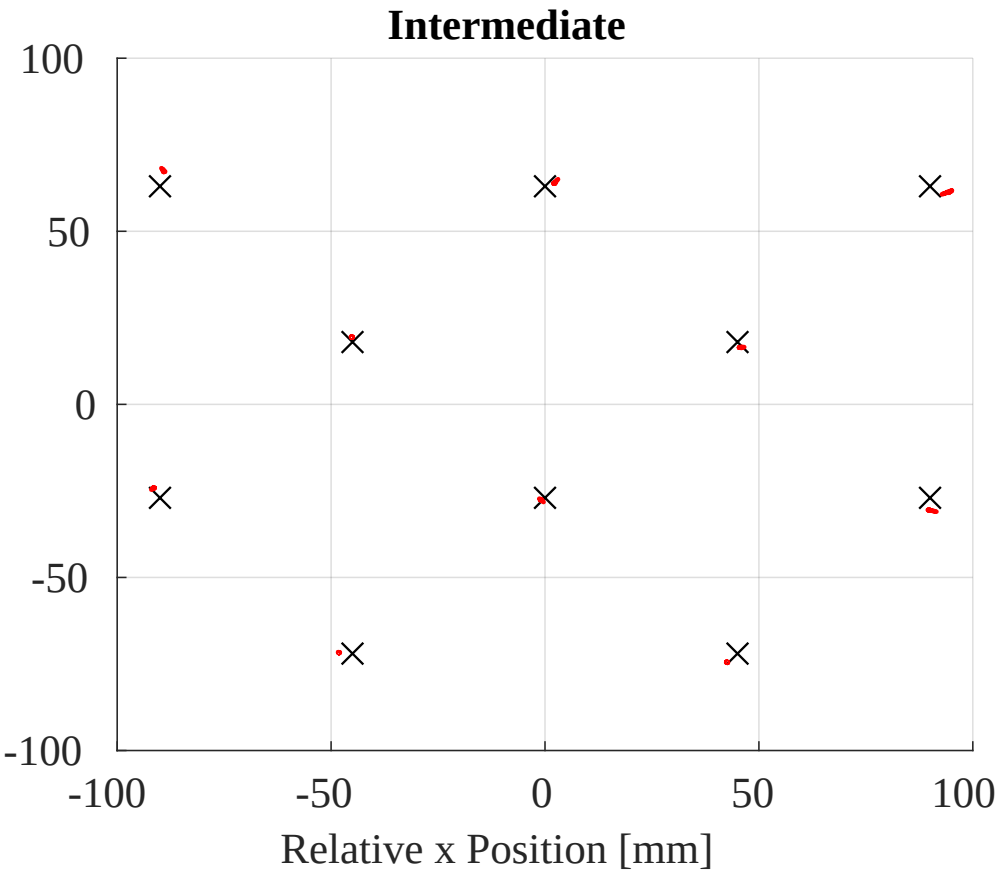

Figure 5.8: Depicts the relative accuracy in the XY plane relative to the ArUco grid. The ground truth (X) is compared with the measured output from the computer vision algorithm. This is shown for the intermediate configuration.

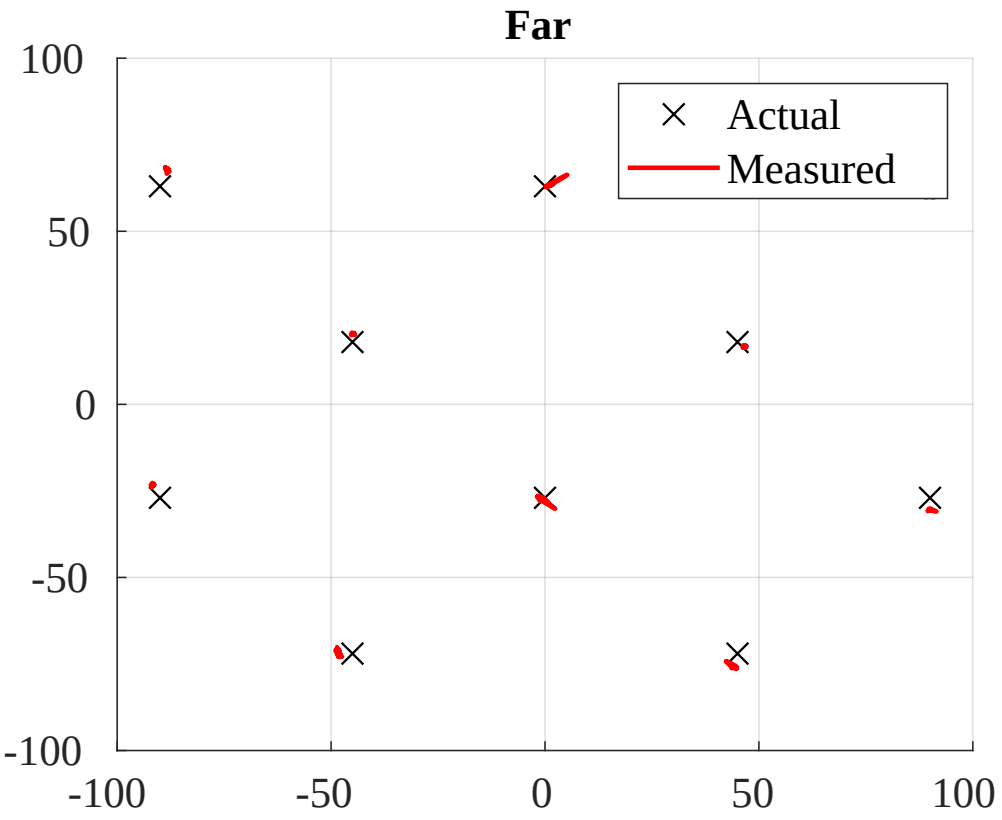

Figure 5.9: Depicts the relative accuracy in the XY plane relative to the ArUco grid. The ground truth (X) is compared with the measured output from the computer vision algorithm. This is shown for the farthest configuration.

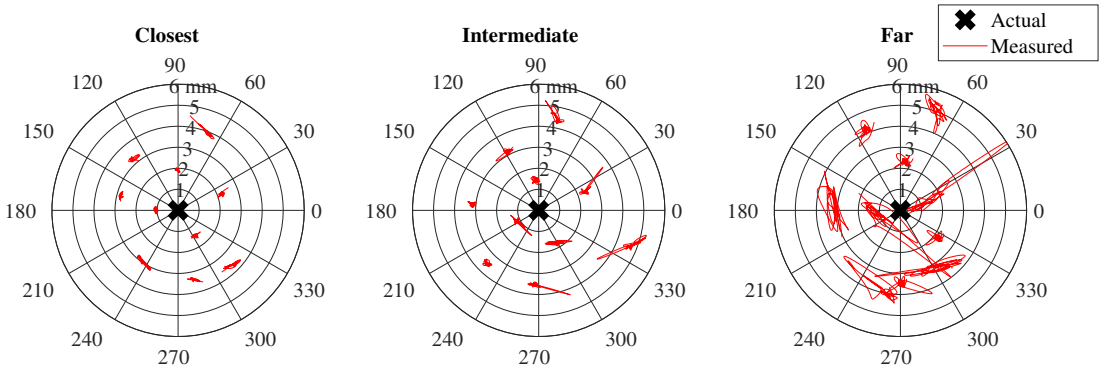

Figure 5.10: A magnified view of fig. Fig. 5.7 with all ground truth points aligned at the origin.

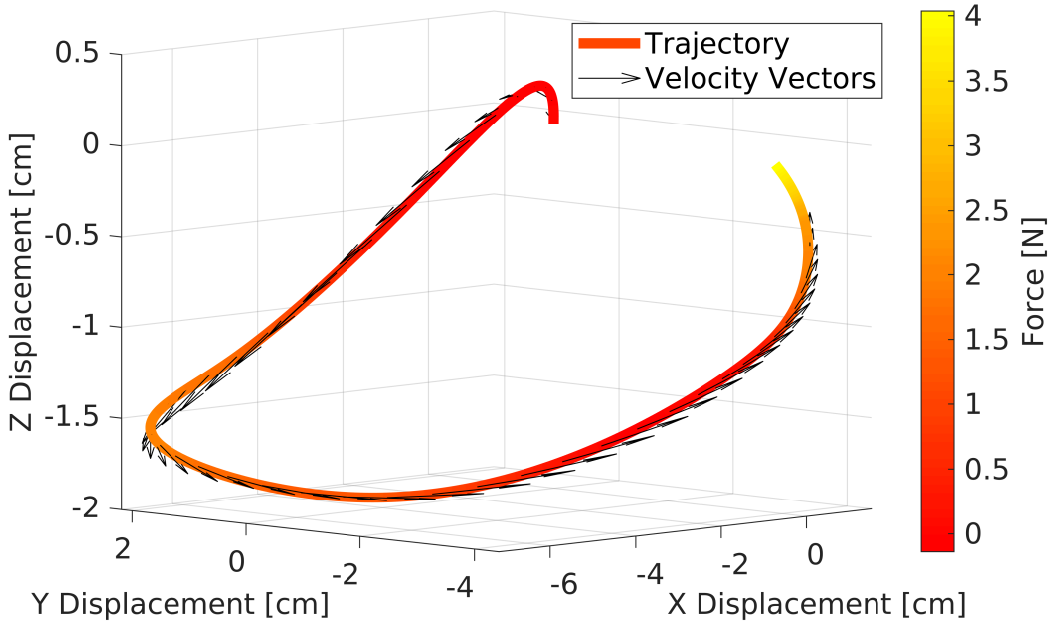

Figure 5.11: 3D trajectory captured during the cadaveric study. Represents motion and dynamics of catheter insertion force assessment tool over a 2 second period.

5.6 EUS 2019 Abstract

Included on the next page is the author's abstract submission to the 2019 Engineering and Urology Society meeting.

ABSTRACTS

ABSTRACT 21

Dynamics of Foley Catheter Insertion: A Cadaver Study

Xiaoyin Ling[1], Michael B. Tradewell[2], Amer Safdari[2], Robert M. Sweet[3], Timothy M. Kowalewski[1]

University of Minnesota, Department of Mechanical Engineering[1], Biomedical Engineering[2]
University of Washington, Department of Urology[3]

Introduction: Catheter associated urinary tract infection (CAUTI) is among the most common non-payment hospital acquired conditions. Foley catheter placement has been shown to impact CAUTI rates [PMID20156062]. Notably, inexperienced healthcare providers such as medical students are associated with a 4-fold higher CAUTI rate [PMID30145285]. Little is known about the mechanical dynamics of urinary catheter insertion. Our objective is to characterize the mechanics of Foley catheter insertion to aid the creation of accurate training modules and simulators.

Methods: The mechanics of Foley catheter insertion were characterized with n = 8 unfixed male cadavers (access through University of Minnesota Medical School Anatomy Bequest Program) and n = 4 simulators. 16f Foley catheters were attempted across all 8 donors. A 16f Coude catheter was used when the Foley was unsuccessful due to prostatic obstruction. Custom designed instrumentation, with a calibrated ± 2 mN accuracy, was used to measure the insertion force [Fig. 1]. OpenCV ArUco markers were used to capture the 3D insertion motion with a GoPro camera.

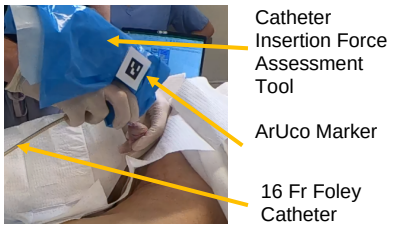

Figure 1: Device and motion tracking marker used during cadaveric procedure.

Results: Out of the 8 donors, only 5 yielded successful catheterizations; all simulator insertions were successful. Greater insertion forces were observed in the simulators. Insertions in the prostate region were also correlated with higher force compared to the distal urethra [Fig. 2]. Both results were statistically significant. Additionally, procedure times were found to be longer for simulator catheterizations (75s mean for simulators, 35s for donors) although this was not statistically significant.

Conclusion: The coupled force measurements and computer vision motion capture gives a first-of-its-kind full mechanic assessment of urinary catheter insertion. With future efforts, we plan to replicate this work in living patients to compare to these cadaveric results and to inform the creation of accurate training modules and simulators.

Acknowledgement: The authors wish to thank the individuals who donated their bodies to the University of Minnesota's Anatomy Bequest Program for the advancement of education and research.

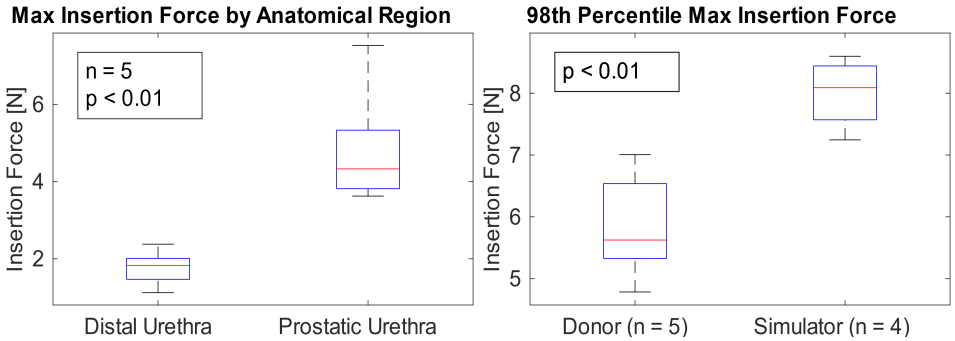

Figure : Summary statistics of donor and simulator experiments.

5.7 Key Results from Cadaveric Study

The catheter insertion force assessment tool was tested on n = 8 cadavers, with only 5 successful catheterizations. Additionally, for comparision the tool was also used to catheterize 2 male mannequins commonly used for training nurses and medical students. Figs. 5.12 and 5.13 show a typical data set from both a cadaveric donor, and mannequin respectively. One contrast between the two is that the simulator data has more frequent, but shorter duration of push events. Additionally, the simulator forces are typically 50% larger than those experienced in the donor tissue.

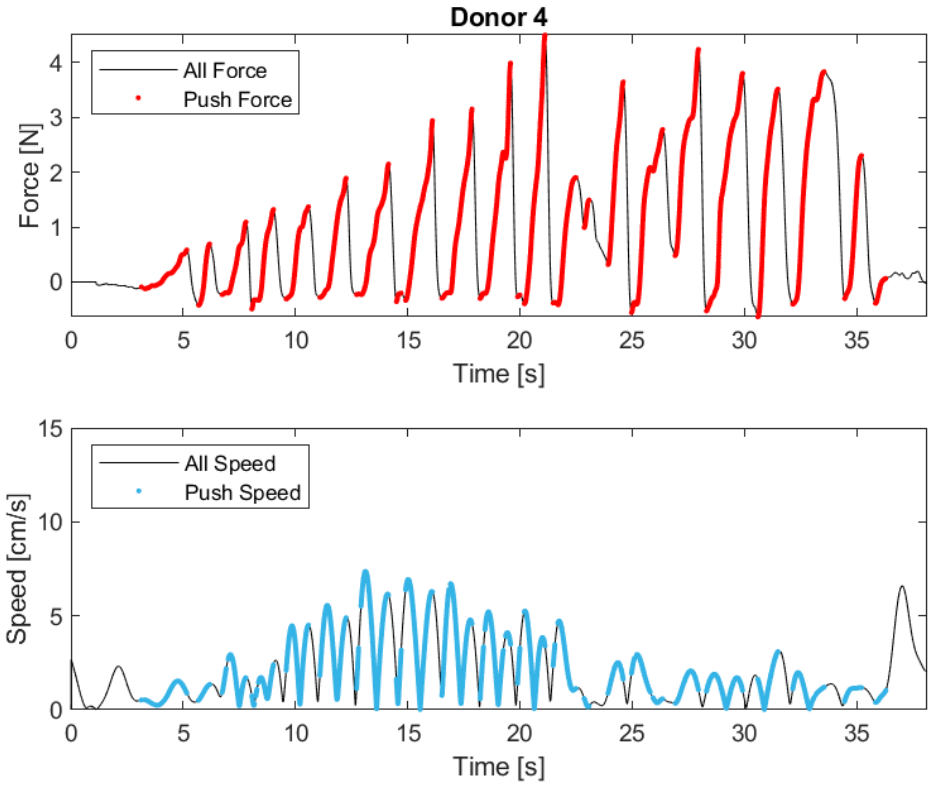

Figure 5.12: Illustrates a representative urethral catheter insertion trajectory including force and speed over the duration of the procedure. This data is from a particular cadaveric donor.

The initial hypothesis when this project was conceived was that the dominant forces

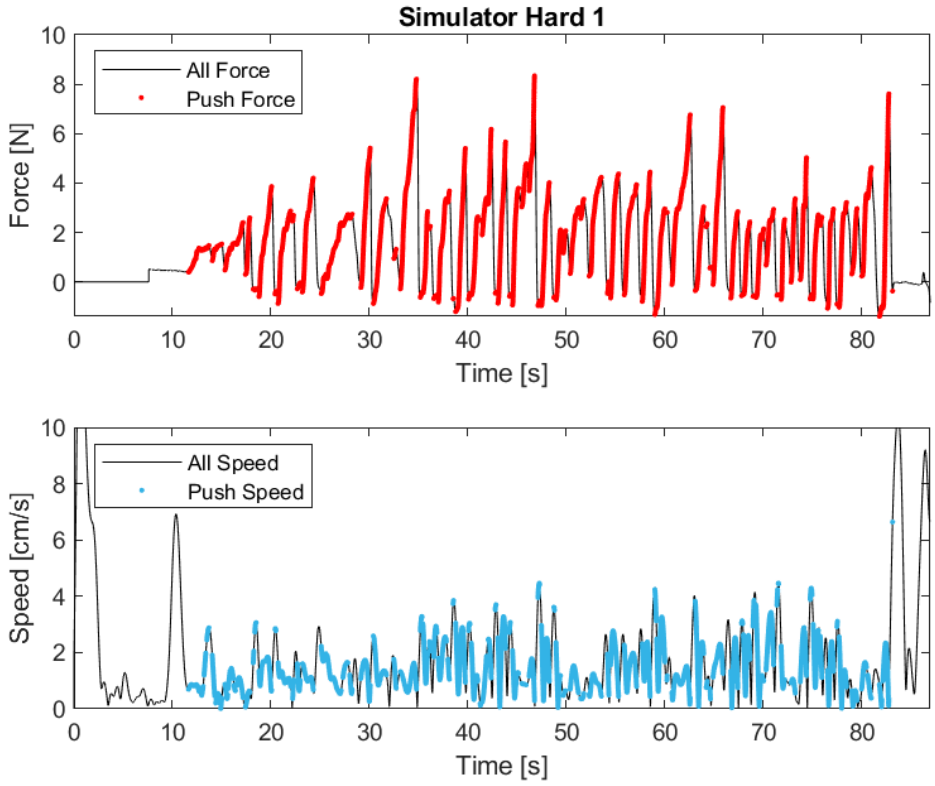

Figure 5.13: Illustrates a representative urethral catheter insertion trajectory including force and speed over the duration of the procedure. This data is from an artificial simulator.

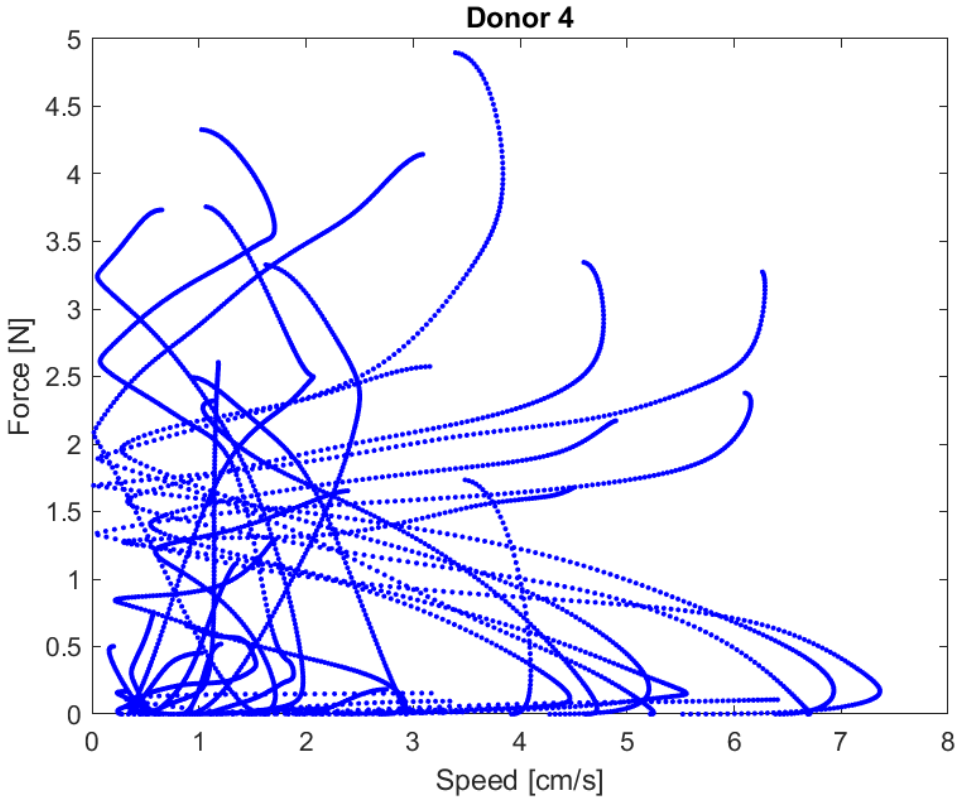

Figure 5.14: Illustrates a representative urethral catheter insertion's force vs speed dependence over the course of a procedure. This data is from a particular cadaveric donor.

encountered during urinary catheterization would be the friction between the catheter-urethra interface. Figs. 5.14 and 5.15 shows the relationship between the insertion forces and speeds plotted against each other. The expectation is that if friction is the dominant force experienced in catheterization, then there should be a trend between the force of insertion and the speed. No such trends can be observed which suggests that there is not a significant influence by friction in the mechanics of urinary catheterization.

The next relationship of interest to investigate is the insertion force vs the insertion length per push event. Figs. 5.16 and 5.17 shows a time series plot of the force as seen previously, under laid with the incremental push length which can be thought of as the integral of the speed during each push event. Plotting these two relations against each

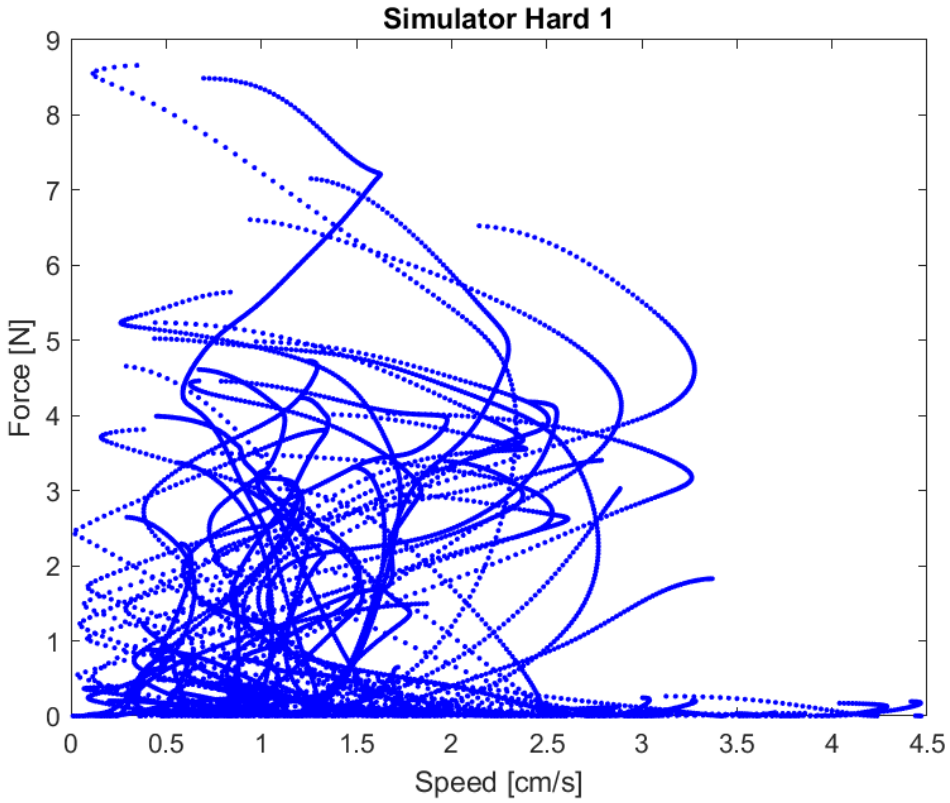

Figure 5.15: Illustrates a representative urethral catheter insertion's force vs speed dependence over the course of a procedure. This data is from an artificial simulator.

other yields Figs. 5.18 and 5.19. Here we find a direct, positive correlation between increasing insertion length and force. Notably the correlation has a bit more spread for the donor tissue, whereas the simulator data is tighter together and more consistent. The existance of this trend between force and length seems to suggest that the physics of urinary catheterization is dominated not by frictional forces, but instead by forces that cause deformation of the local anatomy.

The lack of a frictional dependence when performing urinary catheterization came to the surprise to many of the physicians we have discussed our findings with. The principle objection a few raised was that our experiments only used a single lubrication strategy – that is, we only tested catheterization procedures that had lube applied directly from the catheter tray. An alternative method that is popular, especially for patients that are figured to present a difficulty in passing through the catheter, is to use a syringe to inject the lube directly into the urethra of the patient. Physicians claim that a foley catheter insertion under this method has quite different mechanical characteristics, and they hypothesize that the measured trend would be different and that friction would be the dominant force experienced under those conditions. In future work our group will likely investigate this hypothesis, especially as we move towards in-vivo patient trials.

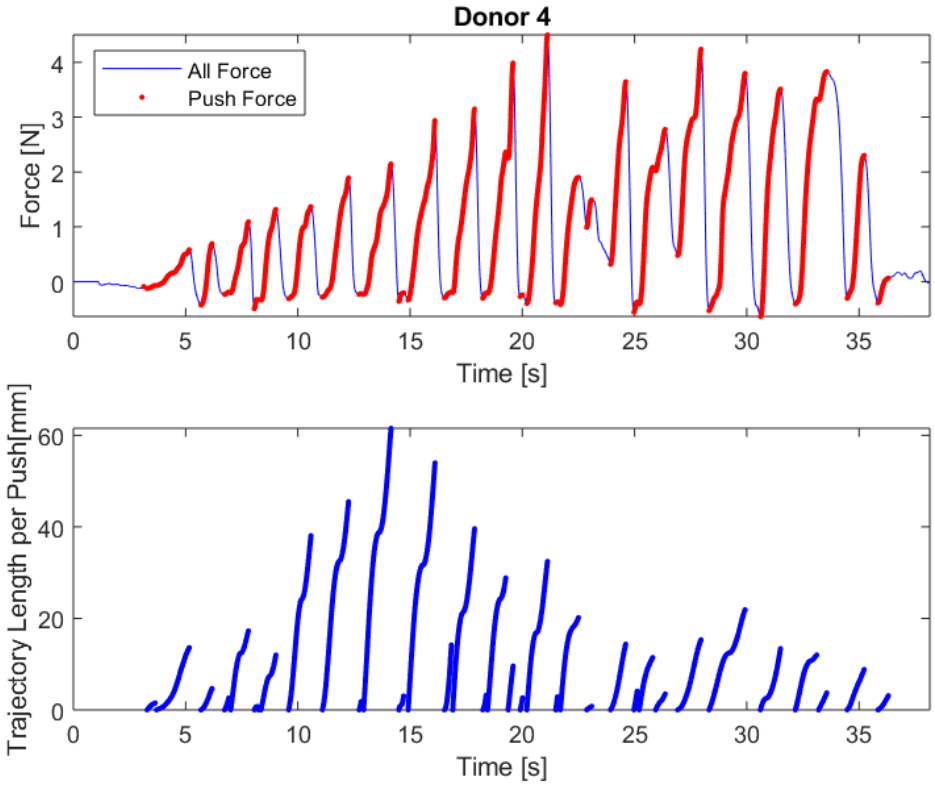

Figure 5.16: Illustrates a representative urethral catheter insertion trajectory including force and push length over the duration of the procedure. This data is from a particular cadaveric donor.

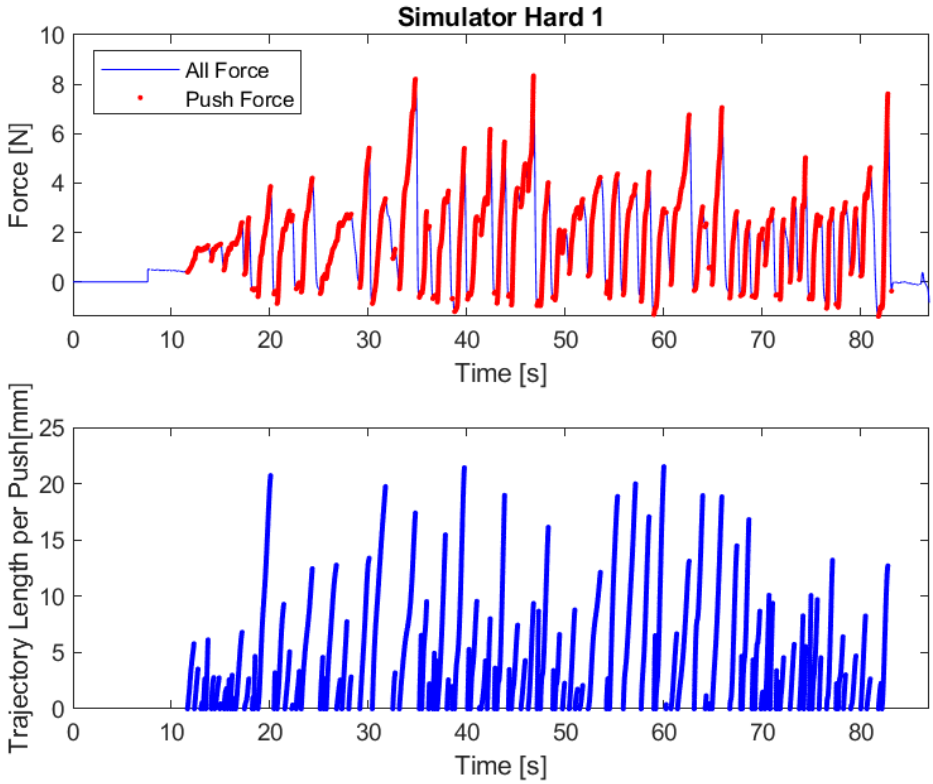

Figure 5.17: Illustrates a representative urethral catheter insertion trajectory including force and push length over the duration of the procedure. This data is from an artificial simulator.

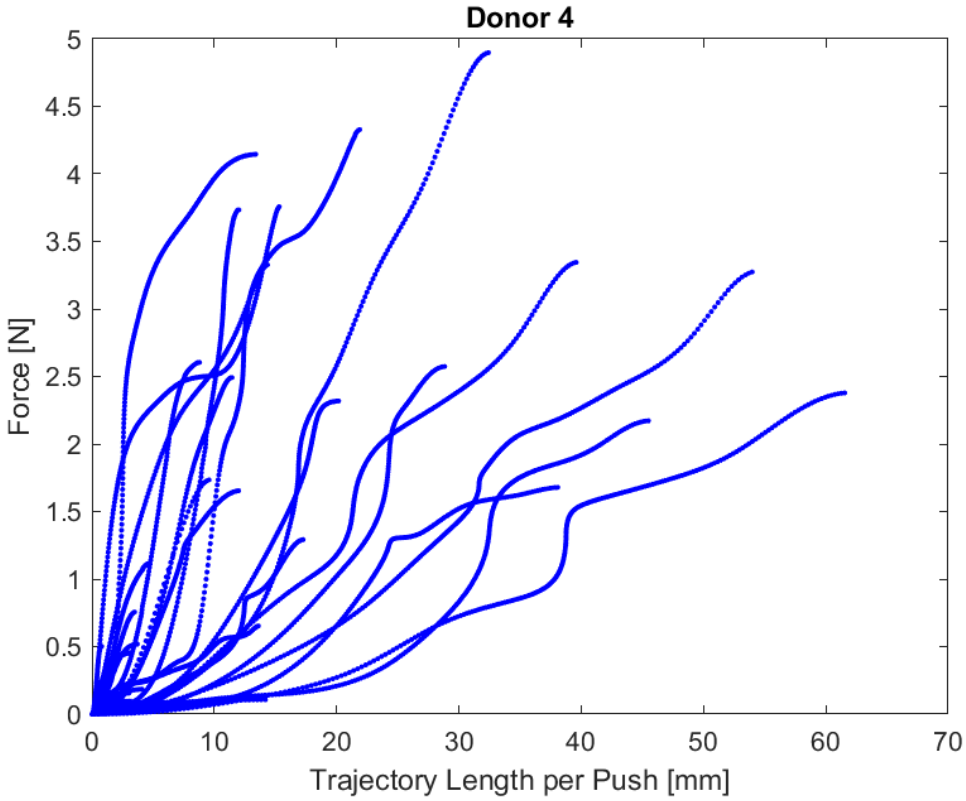

Figure 5.18: Illustrates a representative urethral catheter insertion trajectory including the relationship between force and push length over the duration of the procedure. This data is from a particular cadaveric donor.

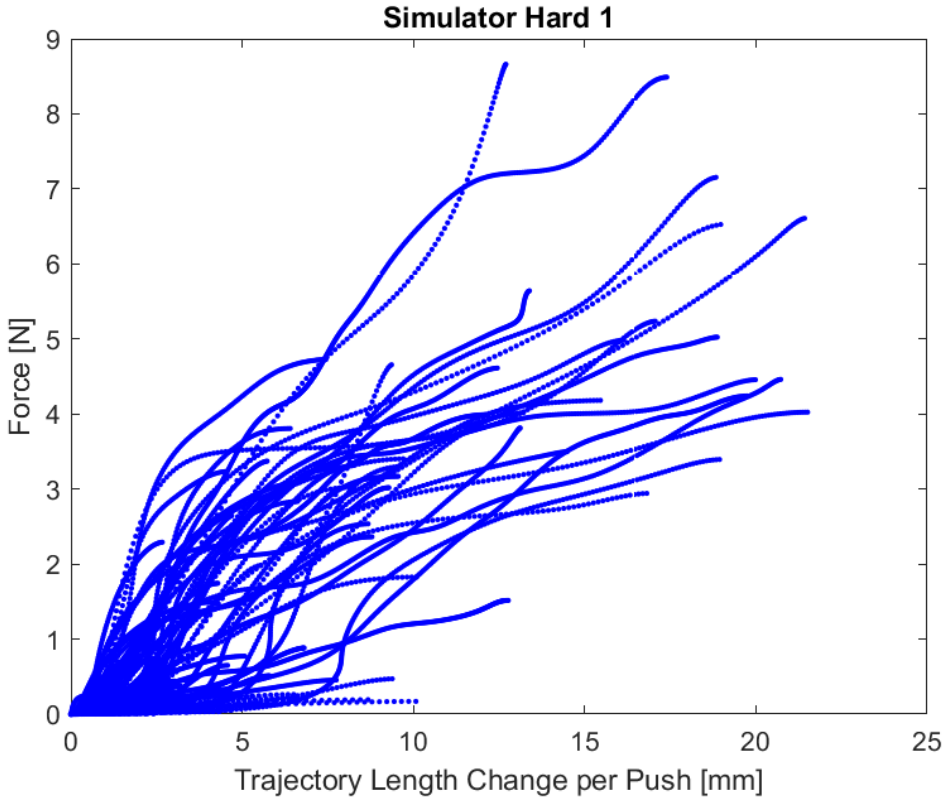

Figure 5.19: Illustrates a representative urethral catheter insertion trajectory including the relationship between force and push length over the duration of the procedure. This data is from an artificial simulator.

5.8 Author's Note

This chapter discussed a brief case study on measuring the mechanics of a particular medical procedure with the intent on using the data to improve the simulator mannequins. The author's primary contribution to this particular work was the measurement of the computer vision performance in motion tracking, collecting and processing the motion data from the cadaveric experiments in addition to assisting with the experiments themselves. Another graduate student, Catherine Ling, was responsible for designing and validating the catheter insertion force assessment tool. This student also took primary lead on analyzing the processed motion and force data. The figures presented in Section 5.7 were originally included in Catherine's thesis and used here with explicit permission.

Chapter 6

Conclusion

6.1 Limitations and Future Work

This work is not without a few significant limitations which limit the scope of the conclusions presented in the results. The first of which is the in-vivo test case was not completed, which was the original objective of this thesis. Aside from that, a big issue with the results is the lack of physical interpretability. A fair amount of this stemmed from the arbitrarity of the data analysis strategies – the choice of curve fit and L-M-H strains were fundamentally arbitrary and its possible to draw completely different conclusions had they been chosen differently. The ideal solution to gain physical interpretability is to further develop the finite element model and inverse solving pipeline which unfortunately was not working at the conclusion of this thesis. Additional work and literature review into reducing the arbitrarity of the other two analysis paradigms would also be a direction for future work.

The inclusion of the human element in the testing process, specifically the manual grasping, did add an element of variability that was not completely accounted for in the experiment and analysis. This in effect has grasps which cause variable strain rates to the tissue. One justification for this is that it realistically tests tissues in the viscoelastic regieme that a typical physician experiences. From a scientific standpoint however, it limits the repeatability of the results but also introduces variability in the results. Future work should seek to reduce or eliminate this, but also taking viscoelasticity into account in the analysis would be very fruitful.

One aspect to the analysis that is completely left unanswered is the lack of an ability to quantify the practical significance of the changes in the parameters of interest. The original intention was to quantify a percent difference in the various parameters and only report those that also are statistically significant – however in examining some of the differences, it was deemed to be largely misleading. If the a coefficient changes by 50%, but the toe regions are largely unchanged at the low strain regime – is it correct to tell our sponsors that tissues change up to 50% under various conditions? Future work should investigate measures of practical significance that aligns with the use of statistical significance.

The last limitation that comes to mind is that in the preliminary study, only 2 tissues were tested. Furthermore, the two that were tested were both highly cellular with the liver also highly vascularized. Care should be taken not to generalize the conclusions in this thesis to other tissues, especially those that are more acellular and/or weakly vascularized as the effects of dissection and freezing are likely to be drastically different.

6.2 Final Remarks

This thesis began with a brief introduction to the problem, and an outline of the research objective. To reiterate, the objective was to measure and compare the mechanical responses of porcine tissues from in-vivo to ex-vivo across common testing modalities. The purpose for this research was to aid in the development of next generation medical simulators. While unfortunately the in-vivo case did not make it for the writing of this thesis, despite the setback, a large portion of the research objective was investigated. Chapter 2 provided a description of the design of a device to accomplish this task. Chapter 3 provided a description of the experimental design and data analysis strategies for comparing across the different conditions. Lastly, Chapter 4 provided a set of preliminary results and a brief discussion and interpretation for an n = 4 porcine carcass study.

The major conclusions from that were measurable changes appeared to occur even from in-situ to bench top, filling a gap in existing knowledge. Though no investigation was provided to eucilidate the mechanisms that underlie this phenomenon. The parameter changes seem to suggest a global decrease in stiffness of the tissue; with the nuances

being a longer toe region but sharper strain hardening response. But, no simple single number or characteristic (e.g. % damage) emerges that emcompass and agree with all the analyses presented.

Finally, Chapter 5 returns to the original impetus for the research with a case study on urinary catheterization. While none of these sections directly informed the creation of next generation simulators, it is the authors hope that this research is actively continued so as to ascertain the true discrepancies in in-vivo and ex-vivo tissues such that our next generation of physicians, nurses, and combat medics can experience the most lifelike and realistic training to better prepare them for what lies ahead.

Bibliography

[1] Iman Brouwer et al. "Measuring In Vivo Animal Soft Tissue Properties for Haptic Modeling in Surgical Simulation". In: *Medicine Meets Virtual Reality* (2001).

[2] Benjamin K. Canales et al. "Urethral catheter insertion forces: a comparison of experience and training." In: *International Brazilian Journal of Urology*. Vol. 35. 2009, pp. 84–89.

[3] Tim Dall et al. *The Complexities of Physician Supply and Demand*. Tech. rep. 2019.

[4] Garrido. *OpenCV ArUco Tutorial*. `https://docs.opencv.org/3.4.3/d5/dae/tutorial_aruco_detection.html`. 2015.

[5] Sergio Garrido-Jurado et al. "Automatic generation and detection of highly reliable fiducial markers under occlusion". In: *Pattern Recognition* 47.6 (2014), pp. 2280–2292.

[6] Carolyn V. Gould et al. "Guideline for Prevention of Catheter-Associated Urinary Tract Infections 2009." In: *Centers for Disease Control and Prevention*. 2009.

[7] Amy E. Kerdok, Mark P. Ottensmeyer, and Robert D. Howe. "Effects of perfusion on the viscoelastic characteristics of liver". In: *Journal of Biomechanics* 39.12 (2006), pp. 2221–2231.

[8] Yi Je Lim et al. "In situ measurement and modeling of biomechanical response of human cadaveric soft tissues for physics-based surgical simulation". In: *Surgical Endoscopy and Other Interventional Techniques* 23.6 (2009), pp. 1298–1307.

[9] Xiaoyin Ling et al. “A catheter insertion force assessment tool: design and preclinical results”. In: *Engineering and Urology Society 33rd Annual Meeting*. San Fransisco, CA, 2018, p. 28.

[10] Edoardo Mazza et al. “Mechanical properties of the human uterine cervix: An in vivo study”. In: *Medical Image Analysis* 10.2 (2006), pp. 125–136.

[11] Karol Miller. “Constitutive model of brain tissue suitable for finite element analysis of surgical procedures”. In: *Journal of Biomechanics* 32 (1999), pp. 531–537.

[12] Karol Miller et al. “Mechanical properties of brain tissue in-vivo: experiment and computer simulation”. In: *Journal of Biomechanics* 33 (2000), pp. 1369–1376.

[13] A. Nava et al. “In vivo mechanical characterization of human liver”. In: *Medical Image Analysis* 12.2 (2008), pp. 203–216.

[14] S. Nicolle, P. Vezin, and J. F. Palierne. “A strain-hardening bi-power law for the nonlinear behaviour of biological soft tissues”. In: *Journal of Biomechanics* 43.5 (Mar. 2010), pp. 927–932.

[15] Sina Ocal. “Effect of Preservation Period on the Viscoelastic Material Properties of Soft Tissues With Implications for Liver Transplantation”. In: *Journal of Biomechanical Engineering* 132.10 (2010), p. 101007.

[16] OpenCV. *Open Source Computer Vision Library*. `https://github.com/opencv/opencv`. 2018.

[17] Jacob Rosen et al. “Biomechanical Properties of Abdominal Organs In Vivo and Postmortem Under Compression Loads”. In: *Journal of Biomechanical Engineering* 130 (2008).

[18] Amer Safdari et al. “Practical, Non-Invasive Measurement of Urinary Catheter Insertion Forces and Motions”. In: *Design of Medical Devices Conference*. Minneapolis, MN, 2019.

[19] Evren Samur et al. “A robotic indenter for minimally invasive measurement and characterization of soft tissue response”. In: *Medical Image Analysis* 11.4 (2007), pp. 361–373.

[20] Ibrahim Sultan et al. “Impact of Foley Catheter Placement by Medical Students on Rates of Postoperative Urinary Tract Infection”. In: *Journal of the American College of Surgeons*. Vol. 227. 2018, pp. 496–501.

[21] Guangming Zhang et al. “Improved Rubin–Bodner model for the prediction of soft tissue deformations”. In: *Medical Engineering and Physics* 38.11 (2016), pp. 1369–1375.

Appendix A

Additional Figures

A.1 All Grasps

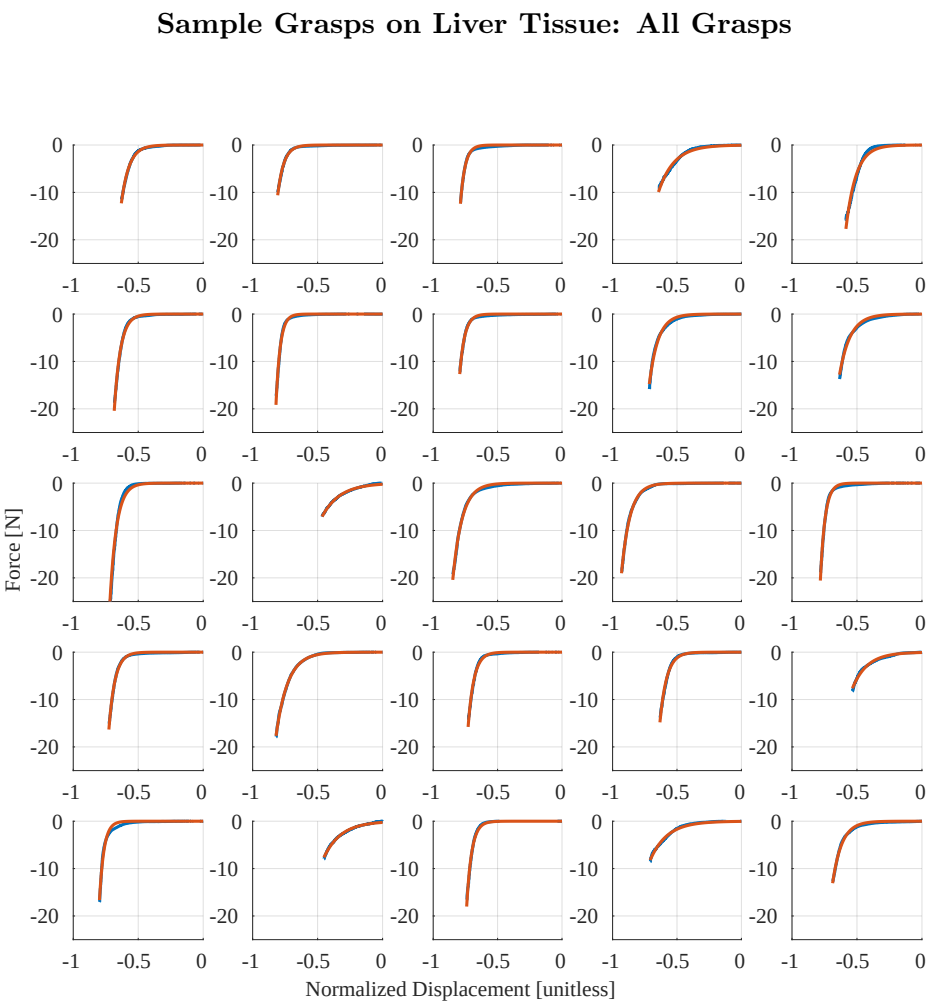

Figure A.1: 5x5 matrix plot of sample grasps on porcine liver tissue. The blue curves represent the actual data, and the orange curve represents the exponential fit.

Exponential Fit Parameters to Liver Tissue: All Grasps

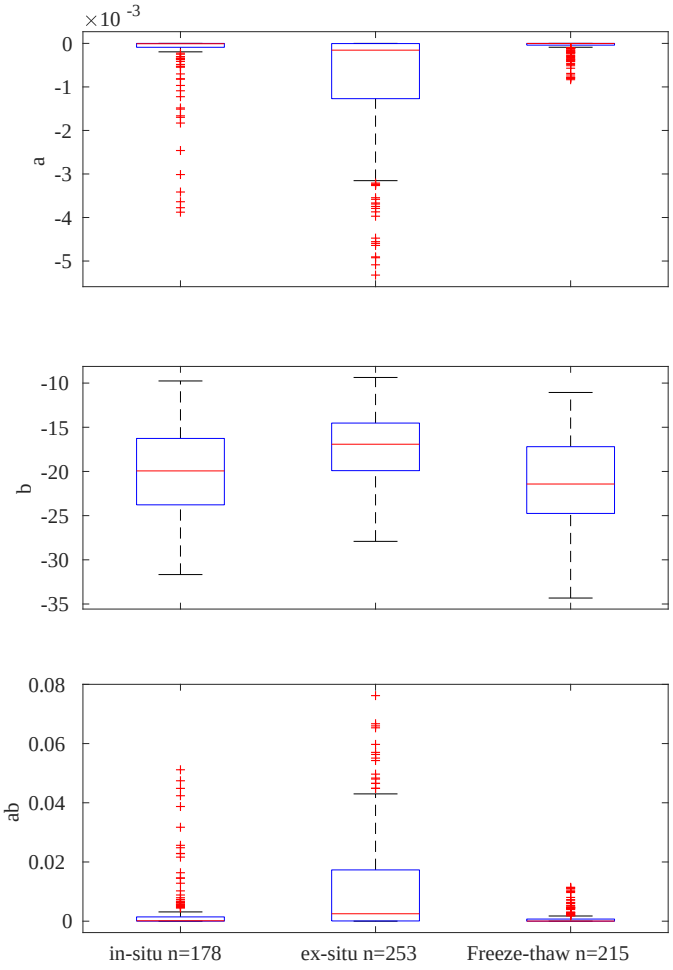

Figure A.2: Box plots illustrating fit parameters for a single term exponential over grasps on porcine liver tissue.

LMH Analysis on Liver Tissue: All Grasps

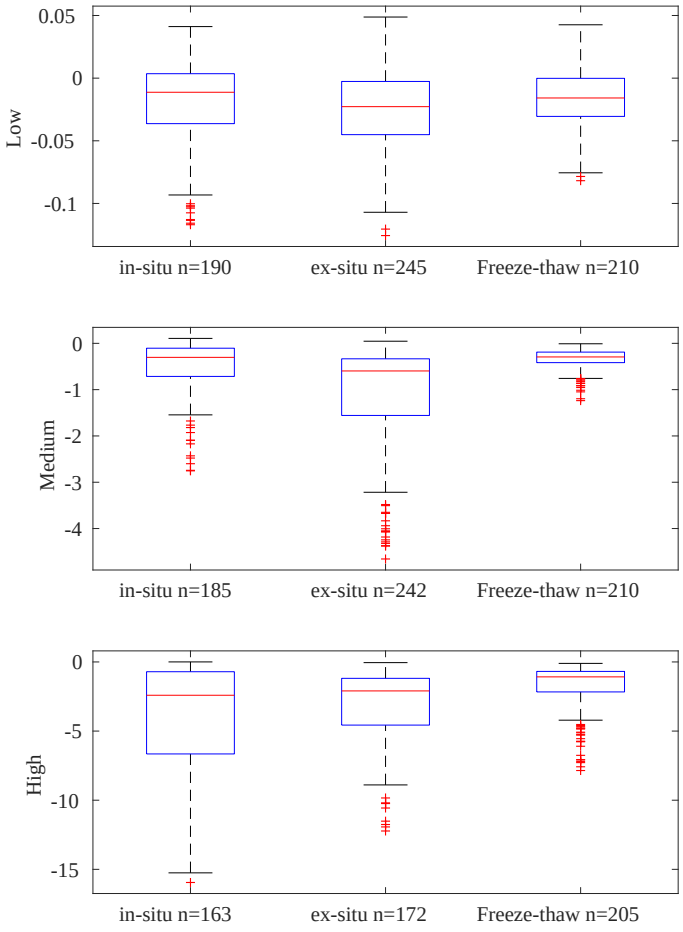

Figure A.3: Box plots illustrating the "Low Medium High" (LMH) analysis of grasp data from porcine liver tissue. These were chosen to be 0.1, 0.5 and 0.65 for the liver, respectively.

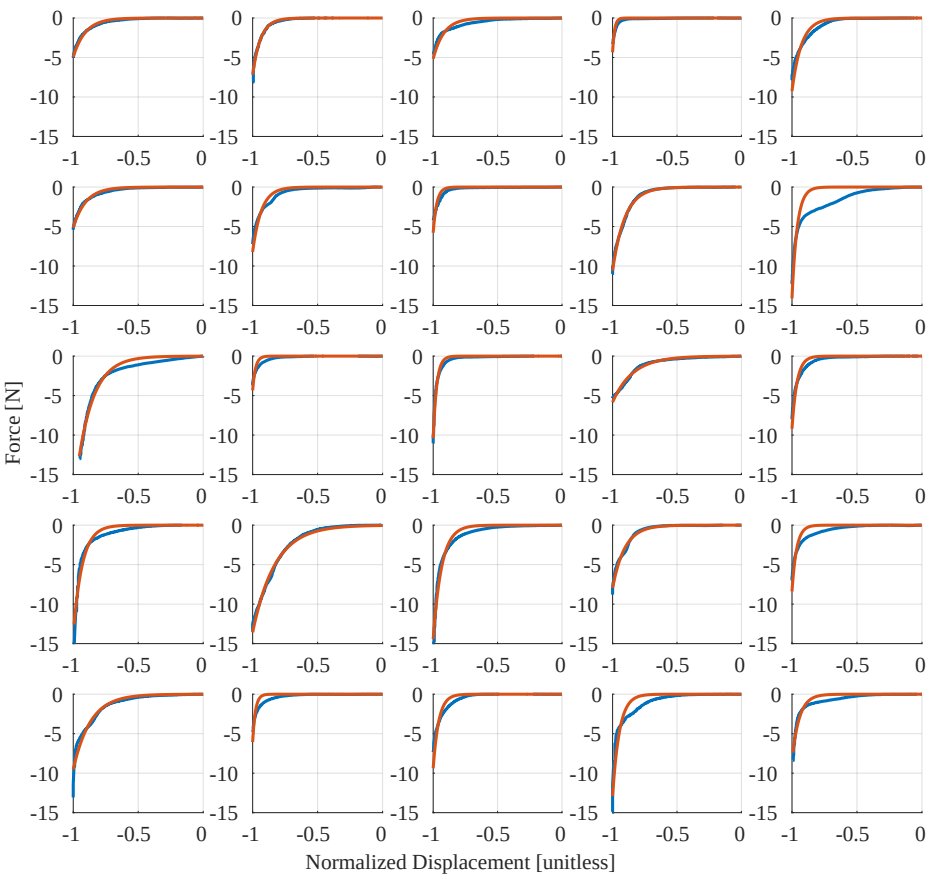

Figure A.4: 5x5 matrix plot of sample grasps on porcine spleen tissue. The blue curves represent the actual data, and the orange curve represents the exponential fit.

Exponential Fit Parameters to Spleen Tissue: All Grasps

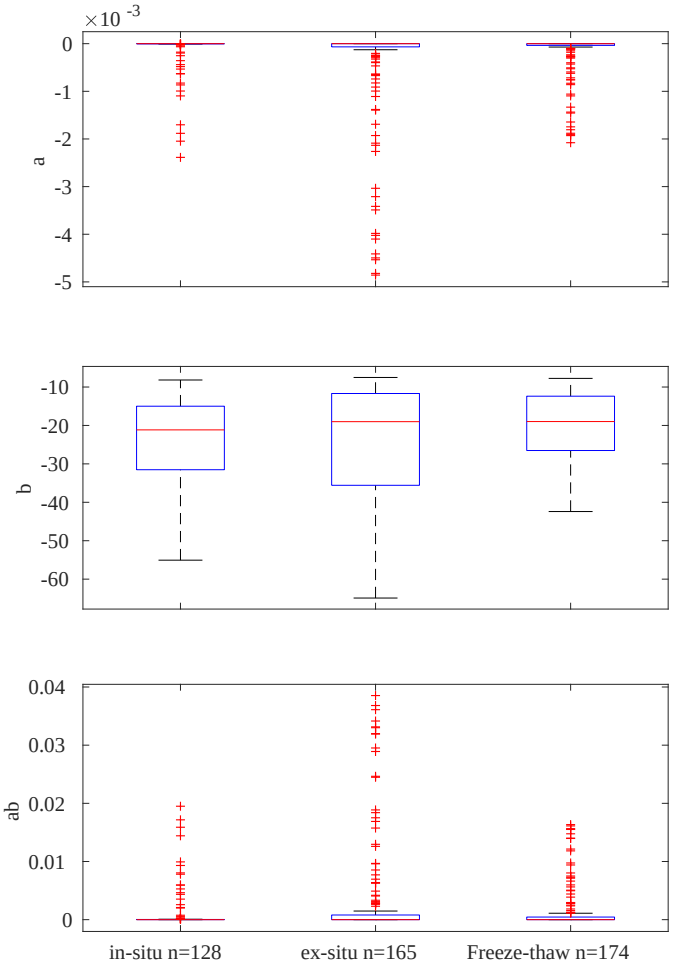

Figure A.5: Box plots illustrating fit parameters for a single term exponential over grasps on porcine spleen tissue.

LMH Analysis on Spleen Tissue: All Grasps

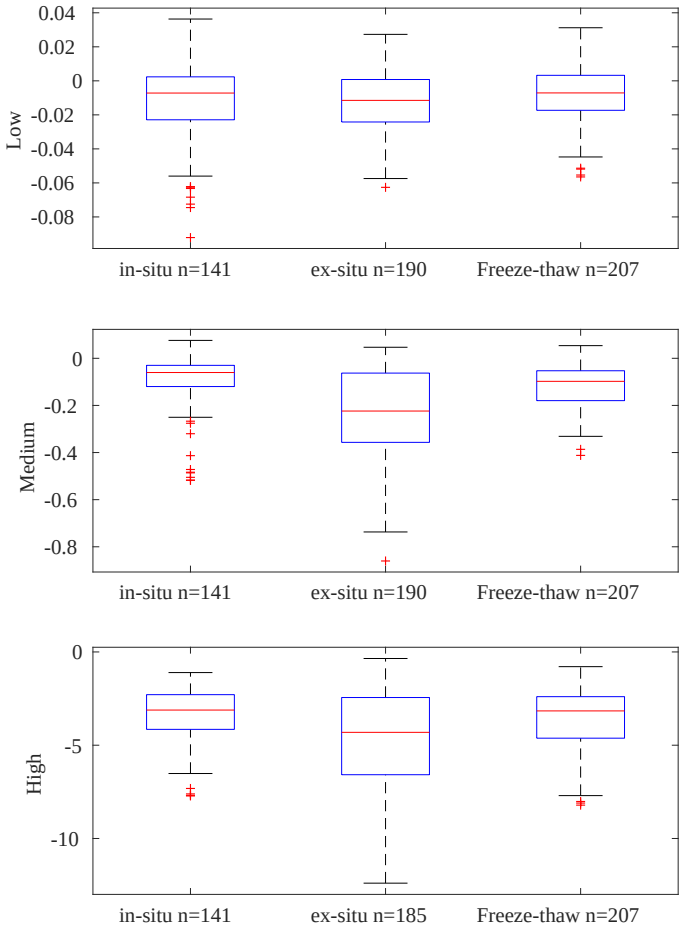

Figure A.6: Box plots illustrating the "Low Medium High" (LMH) analysis of grasp data from porcine spleen tissue. These were chosen to be 0.1, 0.5, and 0.95 for the spleen, respectively.

A.2 Last Grasps Only

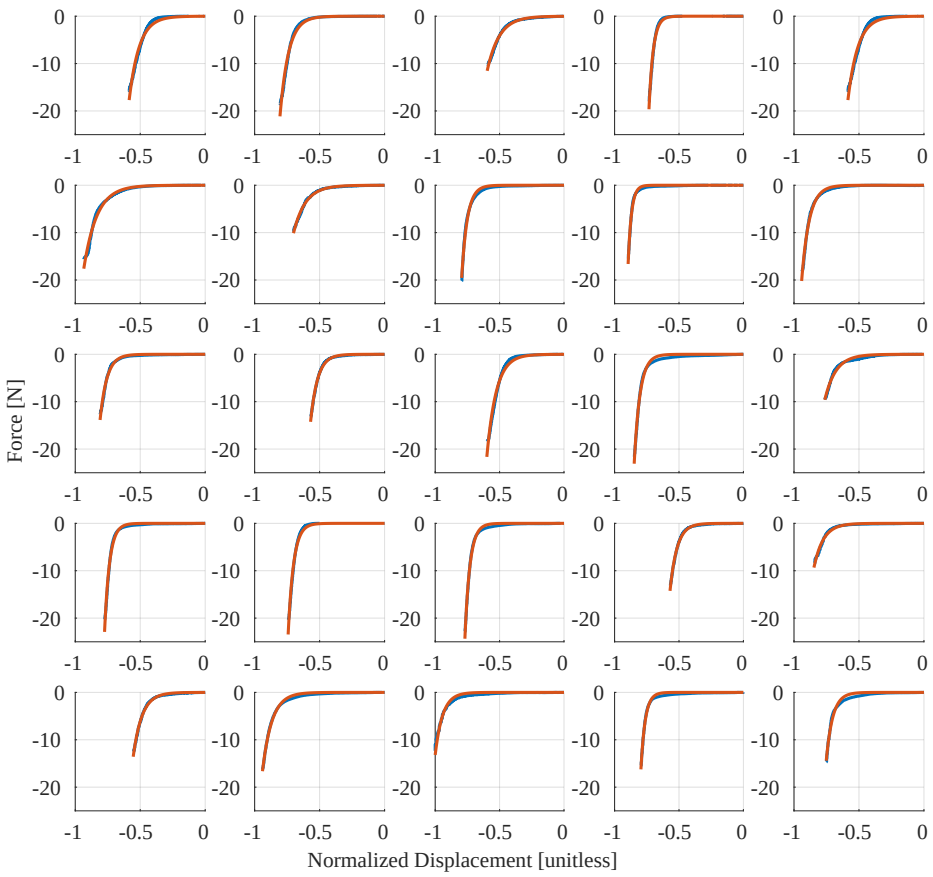

Figure A.7: 5x5 matrix plot of sample grasps on porcine liver tissue. The blue curves represent the actual data, and the orange curve represents the exponential fit.

Exponential Fit Parameters to Liver Tissue: Last Grasps Only

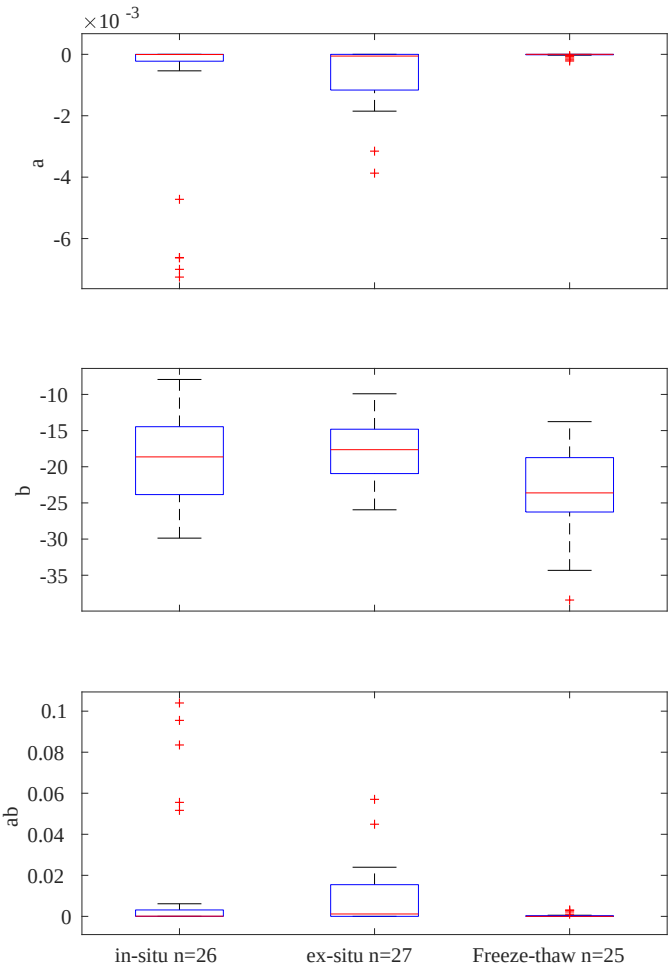

Figure A.8: Box plots illustrating fit parameters for a single term exponential over grasps on porcine liver tissue.

LMH Analysis on Liver Tissue: Last Grasps Only

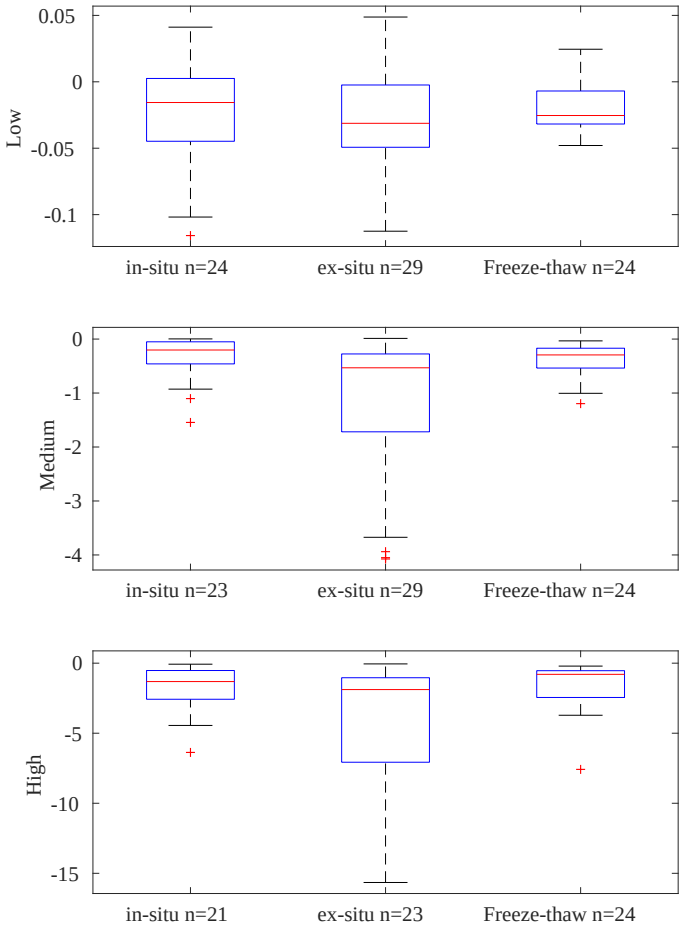

Figure A.9: Box plots illustrating the "Low Medium High" (LMH) analysis of grasp data from porcine liver tissue. These were chosen to be 0.1, 0.5 and 0.65 for the liver, respectively.

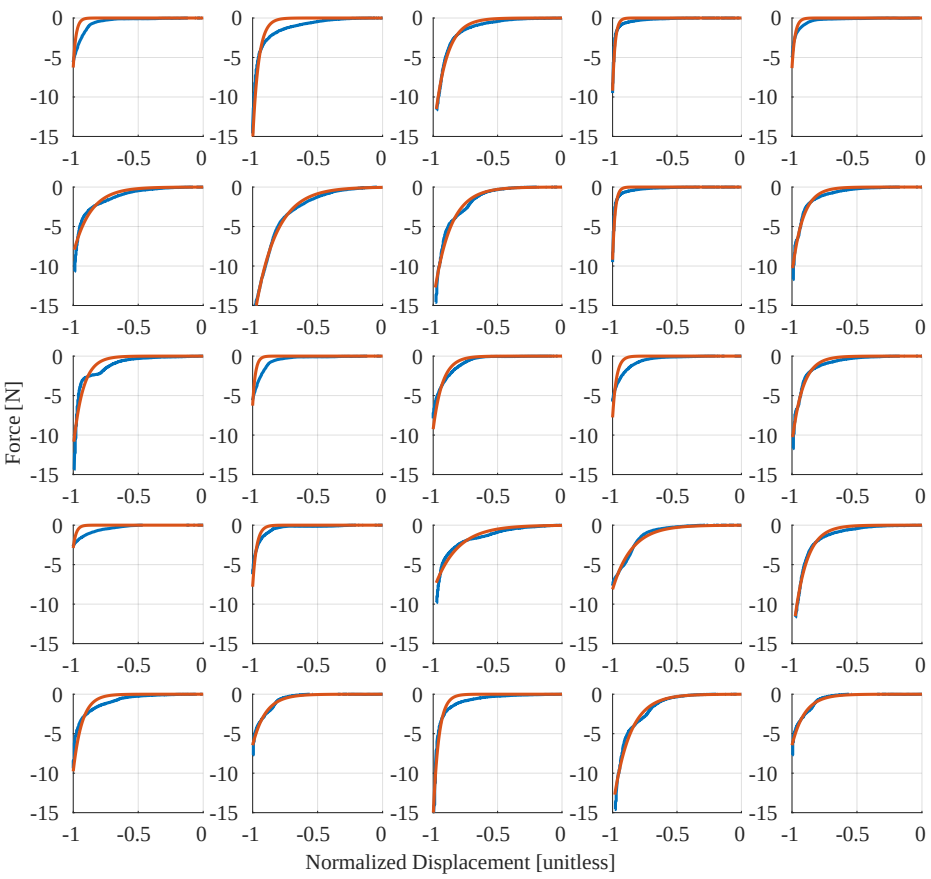

Figure A.10: 5x5 matrix plot of sample grasps on porcine spleen tissue. The blue curves represent the actual data, and the orange curve represents the exponential fit.

Exponential Fit Parameters to Spleen Tissue: Last Grasps Only

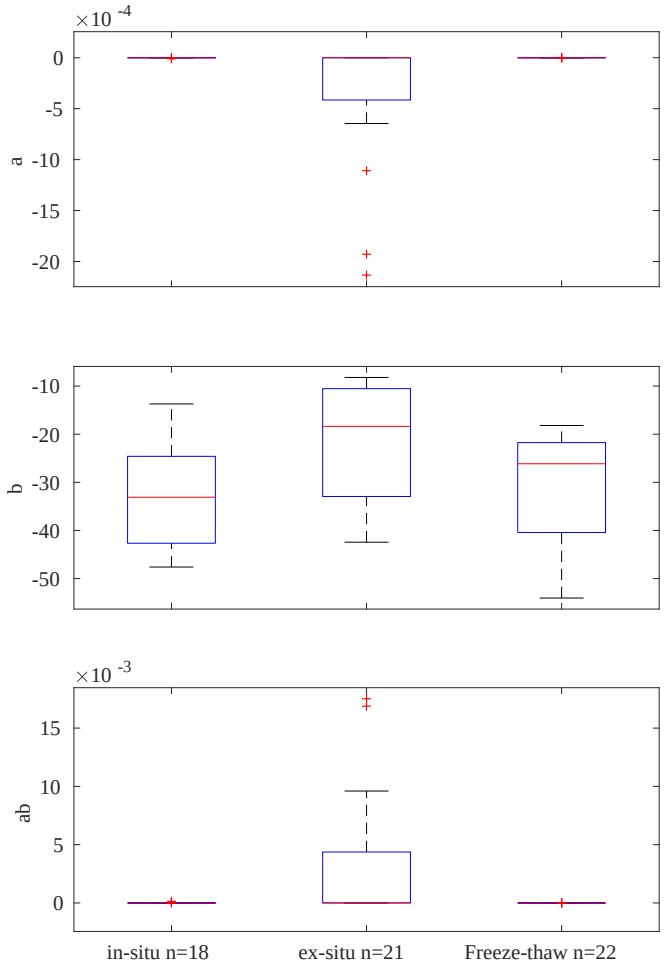

Figure A.11: Box plots illustrating fit parameters for a single term exponential over grasps on porcine spleen tissue.

LMH Analysis on Spleen Tissue: Last Grasps Only

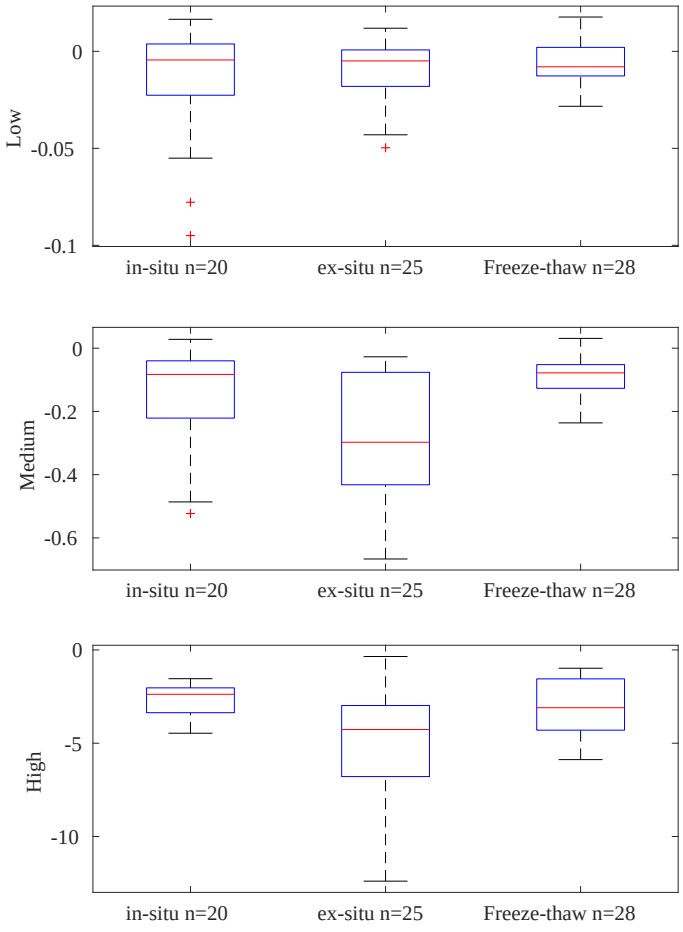

Figure A.12: Box plots illustrating the "Low Medium High" (LMH) analysis of grasp data from porcine spleen tissue. These were chosen to be 0.1, 0.5, and 0.95 for the spleen, respectively.